NRL Memorandum Report 2399

Corrosion- and Creep- Induced Instability-Modeling of Fatigue-Cracking in Various Alloys

J. M. KRAFFT, C. L. LAMB AND K. E. SIMMONDS

Ocean Materials Criteria Branch
Ocean Technology Division

February 1972

NAVAL RESEARCH LABORATORY
Washington, D.C.

DOCUMENT CONTROL DATA - R & D

(Security classification of title, body of abstract and indexing annotation must be entered when the overall report is classified)

1. ORIGINATING ACTIVITY (Corporate author)
Naval Research Laboratory
Washington, D.C. 20390

2a. REPORT SECURITY CLASSIFICATION
UNCLASSIFIED

2b. GROUP
---

3. REPORT TITLE

CORROSION - AND CREEP - INDUCED INSTABILITY - MODELING OF FATIGUE - CRACKING IN VARIOUS ALLOYS

4. DESCRIPTIVE NOTES (Type of report and inclusive dates)
An interim report on this phase of the project.

5. AUTHOR(S) (First name, middle initial, last name)
Joseph M. Krafft, Curtis L. Lamb and Kirth E. Simmonds

6. REPORT DATE
February 1972

7a. TOTAL NO. OF PAGES
58

7b. NO. OF REFS
48

8a. CONTRACT OR GRANT NO.
NRL Problem 84F01-03.101

b. PROJECT NO.
P.O. RR023-03-45-5450

c.

d.

9a. ORIGINATOR'S REPORT NUMBER(S)
NRL Memorandum Report 2399

9b. OTHER REPORT NO(S) (Any other numbers that may be assigned this report)

10. DISTRIBUTION STATEMENT
Approved for public release, distribution unlimited.

11. SUPPLEMENTARY NOTES

12. SPONSORING MILITARY ACTIVITY
Department of the Navy
(Office of Naval Research)
Washington, D.C. 20360

13. ABSTRACT

Crack propagation, the terminal phase in many mechanical-strength failures, is often deleteriously accelerated by environmental corrosion effects. Data to characterize such effects is costly to obtain, particularly if the thresholds of fatigue and corrosion sensitivities are to be defined. Accurate predictive models are needed to extend the available data base and thus its utility in corrosion engineering. This model attempt ascribes the crack growth to the necessity to maintain a state of tensile stability at the crack tip. Discretely sized crack-tip micro-ligamants (d_T) are assumed to control; they are strained by the loading of the crack; when the loading ceases their stability is upset by creep stress relaxation and by surface corrosion; it is restored to equilibrium by an increment of extra straining which requires crack growth. Stress corrosion and fatigue crack propagation data on some 13 alloys has been culled from the literature and uniaxial and cyclic flow properties measured for each. The correlations are encouraging and suggest ways of predicting the growth thresholds as well as a beneficial effect of section thickness on the limiting strength.

14 KEY WORDS	LINK A		LINK B		LINK C	
	ROLE	WT	ROLE	WT	ROLE	WT
Fatigue crack propagation						
Corrosion fatigue						
Stress corrosion cracking						
Threshold, fatigue						
Threshold, stress corrosion cracking						
Low cycle fatigue						
Plastic instability model						

CONTENTS

ABSTRACT

Crack propagation, the terminal phase in many mechanical-strength failures, is often deleteriously accelerated by environmental corrosion effects. Data to characterize such effects is costly to obtain, particularly if the thresholds of fatigue and corrosion sensitivities are to be defined. Accurate predictive models are needed to extend the available data base and thus its utility in corrosion engineering. This model attempt ascribes the crack growth to the necessity to maintain a state of tensile stability at the crack tip. Discretely sized crack-tip micro-ligaments (d_T) are assumed to control; they are strained by the loading of the crack; when the loading ceases their stability is upset by creep stress relaxation and by surface corrosion; it is restored to equilibrium by an increment of extra straining which requires crack growth. Stress corrosion and fatigue crack propagation data on some 13 alloys has been culled from the literature and uniaxial and cyclic flow properties measured for each. The correlations are encouraging and suggest ways of predicting the growth thresholds as well as a beneficial effect of section thickness on the limiting strength.

PROBLEM STATUS

This report is a draft of a paper to be presented to the 3rd International Congress on Materials in the Sea, Gaithersburg, Maryland, 2-6 Oct. 1972, prepared for advanced discussion by ASTM Committee F.24/4 meeting in Philadelphia, 7 March 1972. Work on the general problem of corrosion of materials in the sea is continuing.

AUTHORIZATION

This work was supported by the Office of Naval Research, Project Order RR023-03-45-5450, NRL Problem F01-03.101.

CORROSION-AND CREEP-INDUCED INSTABILITY-MODELING OF FATIGUE-CRACKING IN VARIOUS ALLOYS

INTRODUCTION

Engineers are trained to treat fatigue in terms of the S-N diagram; stress corrosion in terms of the failure time of stressed smooth specimens. The difficulty here is that no useful distinction can be made between cycles or time to initiate a crack, and that for propagation to terminal failure. Experience with smooth specimens usually shows the propagation portion to be relatively short, thus hardly worth discriminating. Yet increasingly it is found that the failure life in real engineering structures is largely propagation time. For example, in cyclic flexing of typically welded bridge girders, Fisher et al (1) find that all of the life is expended in fatigue crack propagation; a nil portion is initiation. The reason appears to be that the stress intensity threshold for fatigue propagation is, after Paris and Bucci (2), so low, that undetectably small crack-like flaws can initiate growth. The thresholds are further reduced by elevated mean stress, the ordinary condition of welded structures. Once a crack has grown to a larger size, Meyn (3) has shown that corrosion effects can greatly accelerate its "progress".

However well we know these generalities, acquiring the data on specific material, loading spectrum and spatial environment combinations is costly and time consuming. Progress could be served by accurate predictive models which permit scant, thus economical data collections to be extrapolated. This paper represents an attempt to establish such a model. It follows an idea proposed by Landes and Wei (4) that creep induced flow can induce tensile instability at a crack tip, and thus crack growth. It

expands a subsequent attempt (5) to apply this concept to transient creep in cyclic loading.

CREEP-CORROSION INDUCED INSTABILITY

Before considering how creep and corrosion can induce tensile instability, it is well to recall how ordinary tensile extension brings it about. An instability may occur at the point in tensile loading at which no further increase in load P is required to continue the deformation; it is the maximum load point, or ultimate tensile strength, or "necking" strain, of the familiar tensile test. If we normalize this load over the supporting sectional area A

$$P = \bar{\sigma} A \tag{1}$$

where $\bar{\sigma}$ is true stress, a function of strain ϵ, then

$$\frac{dP}{d\epsilon} = \bar{\sigma} \frac{dA}{d\epsilon} + A \frac{d\sigma}{d\epsilon} \quad . \tag{2}$$

The ratio of the areal strain differential dA/A to that of longitudinal strain $d\ell/\ell (= d\epsilon)$ is proportional to Poisson's ratio ν, $dA/d\epsilon = -2\nu A$. Designating the true strain hardening rate as $\bar{\theta}$, the condition for tensile instability, $dP/d\epsilon = 0$, becomes

$$\frac{\bar{\theta}}{\bar{\sigma}} = 2\nu \tag{3A}$$

or approximately unity for incompressible plastic flow where $\nu = 0.5$. In simple tension where the tangent modulus $\theta_T = (\bar{\theta} - \bar{\sigma})$ and, for small strains, $\bar{\sigma} = \sigma_T (1+\epsilon) \simeq \sigma_T$,

$$\frac{\theta_T}{\sigma_T} = 0 \tag{4A}$$

is the instability condition, which occurs then when the tensile curve reaches zero slope, $\theta_T = 0$.

Williams and Turner (6), and Clausing (7) have argued that the instability of material close to a crack tip will be influenced by the locally triaxial stress state. The way of estimating this effect from simple tensile data as proposed by Sachs and Lubahn (8,9) is employed here, where for the maximum degree of triaxiality the instability is suppressed until the strain hardening rate $\bar{\theta}$ has decreased to the point where

$$\frac{\bar{\theta}}{\bar{\sigma}} = 0.5 \tag{3B}$$

This means that the strain for fully triaxial instability is larger than that for uniaxial tension of eq. 3A, for which $\bar{\theta}/\bar{\sigma} = 1$. Converting to tension as for eq. 4A

$$\frac{\theta_T}{\sigma_T} = -1/2 \tag{4B}$$

or

$$\frac{\bar{\theta}_T}{\sigma_T} + z = 0; \quad \begin{matrix} z = 0 \text{ uniaxial} \\ z = 1/2 \text{ triaxial} \end{matrix} \tag{4}$$

On the simple tensile curve, this delays the instability until the slope is decreasing with strain at a rate of $-\sigma_T/2$. In materials exhibiting a "flat top" stress-strain curve, as in two maraging steels and one mild steel to be discussed, this delay has a substantial effect in forestalling fast fracture instability.

If straining is interrupted short of the point of tensile instability, as at a crack tip cycled to a K_I level less than K_{Ic} (i.e. subcritical),

the load carrying capacity of a tensile ligament will tend to decrease due to transient creep relaxation. This occurs in ordinary metals even at room temperature. In addition, if the environment is corrosive, the reduction in cross section by surface attack will have a similar effect. As both effects are time dependent it is necessary to express the instability condition in temporal coordinates, whence eq. 2 becomes

$$-\bar{\sigma}\frac{dA}{dt} = A\frac{d\bar{\sigma}}{dt} \tag{5}$$

In tension, the left-hand term of eq. 5 represents strength loss due to sources of areal diminution; the right, increases due to strain hardening but decreases due to creep. Specifically, the areal diminution due to Poisson contraction is expressed as $A(d\epsilon/dt)$, while that due to a corrosion rate V_S (typical units mils/year, in./sec., microns/sec.) is $\pi d_T V_S$ where d_T is the ligament diameter.

The stress relaxation at constant strain is measured directly in these experiments, rather than converted from a measured strain rate sensitivity, $m = d\ln\sigma/d\ln\dot{\epsilon}$, as in the earlier fatigue modeling attempt (5). The transient creep can be characterized by

$$m = -\frac{d\ \ln\sigma_T}{d\ \ln\ t} = \text{constant} \tag{6}$$

where σ_T is the measured decay in tensile stress as a function of time t after sudden arrest of the straining machine. For relatively short hold times of the fatigue cycle, the stress relaxation is

$$\Delta\sigma \simeq m\ \sigma_T\frac{\Delta t}{\tau} \tag{7}$$

where Δt is the dwell time at peak load and τ is Δt plus the loading time t_1, Figs. 1 and 3.

The rationale for converting between measures of strain rate and creep relaxation sensitivities is repeated here from the earlier paper (5) for completeness, Fig. 1. Consider the time required to traverse a path in stress strain space to a fixed strain ϵ at two different strain rates, arriving there with a stress difference, $\Delta\sigma$, approximated by

$$\Delta\sigma \simeq m\bar{\sigma}\,\frac{\Delta\dot{\epsilon}}{\dot{\epsilon}} \tag{8}$$

Substituting $\dot{\epsilon}_1 = \epsilon/t_1$, $\dot{\epsilon}_2 = \epsilon/t_2$ and $\Delta\dot{\epsilon} = \dot{\epsilon}_1 - \dot{\epsilon}_2$,

$$\Delta\bar{\sigma} \simeq m\,\sigma\,\frac{\epsilon/t_1 - \epsilon/t_2}{\epsilon/t_1}\,, \tag{9}$$

and

$$\Delta\sigma \simeq m\sigma_T\,\frac{\Delta t}{\tau} \tag{10}$$

where $\Delta t = (t_2 - t_1)$ may be regarded as the dwell time at load relative to the total loading plus dwell time $t_2 = \tau$. For sinusoidal fatigue loading $\Delta t/\tau$ would be roughly 1/3, for a square wave, 1.0, and for typical waveforms, somewhere between these limits.

Substitution now of the aforenoted sources of strengthening and of weakening in the "temporal" instability equation (Eq. 5),

$$\bar{\sigma}\left(\frac{\pi}{4}\,d_T^{\,a}\,\frac{d\epsilon}{dt} + \pi d_T V_S\right) = \frac{\pi}{4}\,d_T^{\,a}\left[\bar{\theta}\,\frac{d\epsilon}{dt} - \frac{m\sigma_T}{\tau}\right] \tag{11}$$

whence

$$\Delta\epsilon \simeq \left[\frac{4V_S\Delta t}{d_T} + m\,\frac{\Delta t}{\tau}\right]\left(\frac{\theta_T}{\sigma_T} + \mathfrak{Z}\right)^{-1} \tag{12}$$

where the triaxiality factor $\mathfrak{Z} = 0$ for thin sheet, and $\mathfrak{Z} = 1/2$ for thick sections. The instability conditions are expressed in terms of the equilibrating strain increment, $\Delta\epsilon$ of Fig. 1, for its convenient conversion into the crack extension required to cause it, now to be discussed.

CRACK TIP PLASTICITY MODEL

Tensile strain at the crack tip is concentrated by the strain singularity effect. The form of this singularity affects both the magnitude of the strain as well as its gradient in distance. The limits of possible singularly strength, Fig. 2, range from the simple Elastic Analogue (EA) of inverse half power, to the McClintock (10)mode III shear Plastic Analogue (PA) which is of inverse first power of distance into the material r. The stronger singularity is indicated from analyses of Swedlow and Williams (11), Rice and Rosengren (12) and Hutchinson and Hilton (13). On the other hand experimental measurement of Liu (14) and of Kendall and Underwood (15) indicate a persistence of the weaker half-power singularity and present results show little reason to believe otherwise. Accordingly, present calculations are based on the elastic analogue strain singularity.

$$\epsilon = K_I/E\sqrt{2\pi r} \tag{13A}$$

where K_I is the stress intensity factor ($\sim\sigma\sqrt{\pi a}$), E is Young's modulus of elasticity, and, as noted earlier, r is distance from the crack tip into the unfractured material. Rather than some average effect of the entire field, it has been found useful to hinge instability on the conditions over a fixed small region, very close to the crack tip, idealized as row of tiny tensile ligaments of diameter d_T. The degree of ligament extension in the first (quarter) cycle of loading is taken then as simply

$$\epsilon_T = K_I/E\sqrt{2\pi d_T} \tag{13B}$$

In subsequent cycles of loading ΔK, some of the K-induced excursion in tensile strain will be lost in the obstruction to crack reclosing, and thus to d_T-ligament full strain reversal, due to the residual crack tip plasticity.

A model for this effect will be discussed in the next section; suffice it here to define its magnitude as ϵ_R whence

$$\Delta\epsilon_T + \epsilon_R = \Delta K/E\sqrt{2\pi d_T} \tag{13C}$$

The straining of d_T ligaments resulting from the advancing crack tip, at constant loading (K_I), is a function of the local strain gradient. In prior attempts to explain constant-K subcritical (of K_{Ic}) fracturing (16), this gradient was taken as the non-zero portion of the derivative of the strain singularity

$$\Delta\epsilon = \frac{\epsilon_G}{2d_T}\,\Delta a \tag{14}$$

or

$$\frac{\Delta a}{\Delta\epsilon} = \frac{2d_T}{\epsilon_G} \tag{14A}$$

where ϵ_G, for "gradient strain", represents the K_I- proportional strain level existing at $r = d_T$. Irwin (17) has pointed out that the result using the McClintock plastic analogue singularity form differs from the elastic analogue result only by a multiplicative constant, not in functional form. The K-proportional ϵ_G effect when substituted in the instability equation (12),

$$\frac{\Delta a}{(\Delta N)} = \left[\frac{8V_S\,\Delta t}{\epsilon_G} + \frac{2md_T}{\epsilon_G}\,\frac{\Delta t}{\tau}\right]\left(\frac{\theta_T}{\sigma_T} + z\right)^{-1} \tag{15}$$

tends to depress the growth rate with increasing K_I ($\propto \epsilon_G$) level. On a logarithmic plot, it reduces the slope of the "V-K" plot by -1. A typical fourth power "Paris" relationship between log da/dN and log ΔK is reduced to third power. The effect appears too strong to allow matching the fatigue propagation data. Furthermore, in recent stress corrosion crack velocity

data (18) the K-proportional ϵ_G effect also appears too strong. Thirdly, with the effect (5), the fatigue growth rate should decrease with increasing mean stress, or stress ratio R, while the reverse is generally observed (19). All of these inconsistencies disappear if we regard the gradient strain ϵ_G as a constant of a material, indicative of a constant strength of the strain singularity in the near field of the crack tip. The trend in values of ϵ_G so specified will be seen from the data to be reasonable, though lacking for the present, quantitative modeling. A necessary caveat of such empirical deduction, ϵ_G should be regarded as more nearly constant than proportional to K_I, but not absolutely so.

EFFECT OF MEAN STRESS IN FATIGUE

It is evident from work of Hartman and Schive (20) and of Griffiths, Mogford, and Richards (21) that the overall effect of increased mean stress is an increase in crack growth rate relative to ΔK. Recent results of Paris and Bucci (22) have shown this effect to be magnified at very low ΔK levels, where the zero growth ΔK-threshold is markedly increased with R. The R-effect evidence at hand can be understood as an effect of the crack tip unloading blockage. Once a crack is initially tensioned, unloading cannot fully compress the plastically extended near-tip enclave, or thus d_T-ligament, to its original size, or thus d_T-ligament length. The importance of this effect has been argued by Paris (23), and Rice (24) and substantiated by experimental results of Elber (25).

A model for estimeting the magnitude of the R effect is illustrated in Fig. 3. It is common experience that the crack opening displacement of a precracked specimen returns short of its origin upon unloading.

For a given material, this COD shortage tends to be a constant value, relatively insensitive to the maximum K level. We would assume, as first approximation, this behavior imaged in the strain at d_T, Fig. 3, leaving a characteristic residual ϵ_{RO}. When the m[illegible] K is doubled for the same ΔK (right hand side of Fig. 3) only a part of ϵ_{RO}, proportional to the degree of unloading, is felt, so for given ΔK a larger cyclic strain excursion is experienced in the d_T ligament (lower part of Figure 3). The larger strain excursion results in a decreased terminal value of applicable $\theta_T(\epsilon)$, which via eq. 15, involves a greater crack growth increment Δa. From these considerations the form of ϵ_R for use in Eq. (13C) is simply

$$\epsilon_R = (1 - R)\epsilon_{RO} \tag{16}$$

The value of ϵ_{RO} should be larger for softer materials, and likely reflected by the "hysteresis" loop in load vs COD records for initially precracked specimens. In present results it is simply assigned such value as yields a best fit of the data, as will be apparent later.

Another empirically justified adjustment in the ϵ(at d_T)to K_I relationship is the effect of triaxial stress upon the yield surface. The onset of stress-corrosion-cracking sensitivity is reasoned dependent on the formation of d_T ligaments. Using elastic stress field equations and a Tresca yield condition (16) this requires the K level to be augmented by a triaxiality factor.

$$TF = 1/1-2\nu \tag{17}$$

where ν is the Poisson ratio. Mulherin (16,26) associates the presence of this beneficial effect with the occurrence of a coherent precipitate phase in non-ferrous alloys, as in aluminums, a brass and titanium alloy; its absence with the non-coherent carbide precipitate of steels.

Present results tend to support the validity of this rule, as will be apparent later.

FRACTURE FLOW DIAGRAM CONSTRUCTION

The test of veracity of these modeling concepts is in fitting of experimental fracture data - fatigue crack propagation da/dN, stress-corrosion cracking velocity V, as functions of the stress intensity factor ΔK or K_I - to experimental flow data - the cyclic stress strain curves. The scheme of presentation, Fig. 4, involves the cyclic stress strain curves translated to d_T where the crack tip blockage ϵ_R displaces the $\sigma(\epsilon)$ envelope relative to the strain and K origin. The basic "derived" curve $(\theta_T/\sigma_T - Z)^{-1}$ vs ϵ_T appears at the top half of Fig. 4 to the left in each pair. The first cycle or simple tension result rises first on the left, a result of an unrestricted yield point behavior. The triaxiality factor will offset the early elastic ($\nu < 0.5$) portion of this curve to the right by a constant factor. On the other hand the basic "derived" cyclic curve, is offset by a constant increment ϵ_R rather than a constant factor TF. This gives the appearance of a larger (relative) offset at low ϵ_T levels, increasing the loglog slope visavis ΔK-sensitivity of da/dN.

The extreme lower limit or threshold of fatigue growth is taken to correspond to the elastic proportional limit of the cyclic stress strain curve. This strain increment, as measured from the zero stress axis of the total cyclic curve, is augmented by the elastic negative "toe" of the "hysteresis" loop appropriate to the stress excursion limits,

$$\epsilon_T = \Delta\epsilon + \sigma_T/E \qquad (18)$$

In the elastic range then, $\epsilon_T = 2\sigma_T/E$, whereas the ordinate "flow" plot is, from Eq. 15, essentially σ_T/E, directly proportional to ϵ_T, i.e. equal to $\epsilon_T/2$. The log-log-plot of this is a 1:1 slope of constant ratio X:Y=2:1. This 45° line breaks sharply upward at a strain corresponding to the elastic limit, which aids in its experimental location (i.e. of the growth threshold) from the stress strain curve. For strains, vis-a-vis ΔK in fatigue below this point, the growth rate does not follow the 45° line but goes to zero because the stress relaxation (m) becomes zero for elastic deformation.

The corresponding 45° toe region for the first cycle curve, germaine to stress corrosion cracking and static creep, is on a X:Y=1:1 line when longitudinal stress strain curves are employed and on a X:Y = $1/2\nu$:1≃1.6:1 for present data where diametral strain was measured, and the strain (but not θ_T) corrected to longitudinal values

$$\epsilon_T = \Delta\epsilon + \sigma_T/M \qquad (19)$$

where $1/M = 1/E - 1/\theta_o$, θ_o being the diametral (areal) elastic modulus (i.e. $\theta_o = -d\sigma/dA/A = -2d\sigma/dD/D$). Since the stress corrosion cracking is corrosion rate (V_S) dependent rather than creep (m) dependent, the 1:1 elastic limit line need not signal a threshold of SCC crack growth and there is slight evidence in present results to suggest this.

The top end of the derived curves, Fig. 4, represents "limit loading" conditions. For the first cycle the (triaxial) instability point should correspond to K_{Ic}. In the cyclic result, there is evidence that uniaxial ($\nu = 0$) instability pertains to thin sheets. If the tensile curve is of relatively flat top, a "hesitation" shelf at an ordinate

value of about 2 (i.e. if $(\theta_T = 0\ (\theta_T/\sigma_T + 1/2)^{-1} = 2)$ will forestall the terminal instability. This can be a beneficial effect in some materials, as will be seen in results to follow.

SPECIMEN MATERIAL AND EXPERIMENTAL PROCEDURE

The present objective is to establish a coherent framework for the fairly abundant reservoir of fatigue crack propagation data dispersed through the literature, and much less plentiful stress corrosion velocity data. For each case, the flow behaviors have been carefully measured and assessed with respect to reaching this objective. Criteria of alloy selection included: 1) existence of a sufficient range of subcritical crack propagation data; 2) availability, to the authors, of identical fracture specimen material for tensile specimens; and 3) variety of material to typify a good range of structural alloys. The resulting collection is listed in Table I, along with some of the numerical results of the study. They comprise thirteen alloys: one carbon steel, two stainless steels, three quenched and tempered steels, two maraging steels, two titanium alloys, and three aluminum alloys. In most cases the tensile coupons were cut from pieces of actual fracture specimens or the same plate stock.

The tensile specimens were made small to allow their fabrication from the oft-times small fracture specimen residuals: 0.170 in diameter by 0.500 in. long test section, with 1/2 in. 20 threads/in. (NF) ends. When less than 1/2 inch stock was available, partial threads were employed. The 4340 specimens were smaller, 0.100 D, with 1/4-28 (NF) ends.

The specimens were strained in a small hydraulic testing machine, described elsewhere (27), fitted with an alignment subpress to minimize the

the buckling tendency in compression. A diametral bilobed clip type gage was instrumented with electric resistance foil gage transducers, which with the load signal was recorded with a Hewlett-Packard X-Y recorder. The Tektronix Q-type strain gage preamplifiers employed proved stable enough for the extremely high gains required for the stress relaxation measurement.

Since so much reliance is placed on the detailed shape of the stress strain curve, a note about differences between diametral vs longitudinal strain measurements is in order. Comparative measurements with a knife-edge type longitudinal strain gage were made on a number of the materials. It was observed that the tension portion (only)of the reveresed cyclic curve was identical for longitudinal vs diametral (areal) strain measurement. The elastic part exhibited the proper longitudinal (Young's) modulus; the remainder of the curve as closely similar. This is taken to mean that the cycled material has been bereft of its compressibility: its Poisson ratio is 1/2 in its tension cycle. The compressive elastic moduli appear greater, as expected, as that for the first tension cycle. This result was taken to justify direct use of the convenient diametral gage for the prediction procedure, which requires a longitudinal strain basis (except for SCC as discussed in reference (16)).

The stress relaxation rate was measured by quickly locking the testing machine head and measuring, with grips thus "fixed", the stress decay. Tc eliminate the effect of work hardening due to slight compliance of the test rig external the test section, the relaxation measurements was made in the maximum load region. Q-unit amplifiers rebalanced, the gain

was increased 10-fold, time marks from a Tektronix 181 mark generator superimposed at 1 sec. intervals until 5 seconds after machine arrest, thence at 5 second intervals until the decay in a 5 sec. interval becomes too small to discriminate on the chart. Some of the records (Figs 10-20) show actual decay traces. A plot of average values for each of the alloys is shown in Fig. 5. The m value is calculated from the slope of the linear $\Delta\sigma_T$ vs log t plot using equation (7) in the form

$$m = \frac{\Delta\sigma}{\Delta \log t / 2.303\sigma_T} \qquad (7B)$$

A linear stress vs log time plot is permissible for the characteristically small values of m of ordinary alloys. The m values, or slope $\Delta\sigma/\Delta\log t$, was found to be constant in most cases, but for cases where it decreases with time, m values for both 1 sec. and 10 sec. slope values are recorded in Table I. The m values are reproducible with $\pm$ 5%.

In the presentation of data to follow, the figures are sequenced in the order of Table I and Fig. 5 to retain the categorical ordering of alloys, but this sequence may be violated in pursuit of argument to amass evidence on a particular point. The variation in scale format of the plots is consistent with varied formats employed by the authors of each data set, to which our "flow predictive" plots were easiest to bring into conformance.

A533 TYPE B CLASS I PRESSURE VESSEL STEEL

The intensive research to which this material has been subjected stems from its importance as a nuclear reactor power plant heavy wall pressure vessel material. Specimens were cut from the 12 in. thick

plate, the center region being of fairly uniform properties. Fatigue tests on 1, 2, 3, and 4 inch CTS specimens were undertaken by Clark (28) while on thinner 0.2 inch as well as 1 inch specimens, Paris and Bucci accomplished the feat of establishing the low growth rate region looking for growth thresholds with respect to the stress ratio R. The extraordinary results reported by Paris, Bucci, Wessel, Clark and Major (29), hereinafter designated by "call letters" WPMBC, has done more we believe than any preceding data set to clarify the nature of fatigue crack propagation.

The Fracture-Flow diagram of the WPMBC data, Fig. 6, is coded to distinguish the six stress ratios and two thickness ranges employed. The actual stress strain records, one of several similar test results, is inset along with thus-derived predictive flow curves. The first cycle stress strain curve shows the characteristic upper yield point followed by a strain hardening rate sufficient for a high, about 17%, strain for simple tensile instability. Its rate predictive plot is shown beyond the region obscured by the yield point instability, although as is unfortunately true of most alloys, no stress corrosion cracking data is available for comparison. However, the mechanical instability strain is in reasonable correspondence with K_{Ic} (30), particularly in view of the variations inherent in this property (31) in carbon steels.

The cyclic strain excursions showed a rather steady form below about 6% extension, but thereafter a progressive decrease in range of tensile stability. The second and third cycle shapes are believed to best characterize the crack tip material ductility as the fourth cycle, displaced downward 10 ksi on the record, appears curtailed by imminent necking and

and rupture; the second cycle result is shown. The flatness developed in these cycles has the effect of causing a large separation between uniaxial and triaxial mechanical instability points. Both second and third cycle curves predict a plane stress growth rate infinity in good correspondence with the thinner plate results of Paris and Bucci. With the triaxial correction, Z of Eq. 15 equal to 0.5, both shift to the right to bracket the thick section results of Clark.

The lower end of the predictive curve permits an assessment of the stress ratio (R) effect for the A533B. Values of the ϵ_R-addition required for best fit of the data were judged from a master plot with a set of equally graded $\epsilon_R = 0.0010$ offset increments. Of the values shown, 0.0020 is best fit for R = 0.8,0.0033 for R = 0.5, and 0.0060 for R = 0.1. These along with the remaining data fits are cross plotted in Fig. 7, showing a reasonable agreement with the Eq. 16 and Fig. 3 model prediction, indicating a value of ϵ_{R0} of about 0.0066 for this alloy. The overall form of the reference curve, as derived from the stress strain curves,can be reproduced from independent test and record measurements to about $\pm$ 5% in either direction. After its correction for R effects, the degree of correspondence with the WPMBC data is encouraging.

The typical procedure used for calculating the "disposable" parameters d_T and ϵ_G implied by the matching is typified here with the A533B. A convenient reference point on the flow diagram is chosen. With "English" units used for the working sheets, the coordinates $\epsilon = 1000$ ksi/$\sqrt{2\pi}$ E, and $(\theta_T/\sigma_T+Z)^{-1} = 1.0$ was marked. At match with the da/dN vs ΔK data, the corresponding value ofΔK yields d_T from Eq. 13: i.e. $\sqrt{d_T} = \Delta K/E\sqrt{2\pi}\ \epsilon = \Delta K/1000$; $d_T = \Delta K^2\ \mu$ in. For the ϵ_G values through eq. 15,

assume a typical loading cycle $\Delta t/\tau = 1/2$, whence $\epsilon_G = m\, d_T/da/dN(ref)$. The m value, taken from data as shown in Fig. 5 and Table I is used. If it is not constant, ϵ_G corresponding to both 1 second and 10 second m values is recorded, then cross plotted against the ultimate tensile strength (cyclic and tensile are about the same) in Fig. 8. The match-determined value of d_T is marked on the growth rate scale of each "Fracture-Flow" diagram, and recorded in Table I.

316 and 304 STAINLESS STEEL

From the studies of effects of high temperature neutron irradiation environments by James (32) and by Shahinian (33), the room temperature data are examined in Figs. 9 and 10. The extraordinary strain hardening capacity of these solution-annealed alloys is evident from the cyclic stress-strain curves, inset in the Fracture-Flow diagrams: first cycle instability strains are of the order of 40 to 50%, which with the indicated d_T value would mean a K_{Ic} of 400 to 500 ksi $\sqrt{in.}$ (or $MNm^{-3/2}$), totally unmeasurable. The equilibrium cyclic instability, though still high, is greatly reduced. The ϵ_R shift of 0.008 (i.e. $\epsilon_{RO} = 0.0089$) for the 316, and 0.007 for the 304 brings the prediction into close correspondence with data. These high values of ϵ_R are not unreasonable in view of the initial softness of these materials: a relatively low elastic field outside the yield zone will be available to recompress the cyclicly hardened crack tip region. Like the A533B carbon steel, the "flat-top" cyclic stress strain curves of these alloys leads to prediction of a large separation in ΔK between plane stress and plane strain conditions. However, since the alloys are so soft and tough, and rarely used in thick sections, it is unlikely that the plane strain "bonus" will be realized in practice

nor is it indicated in the fatigue data.

The values of the gradient strain ϵ_G needed to match predictions to data are seen in Fig. 8 to be atypically low; in other words the fatigue crack propagation rate is unexpectedly high. Some of this may be attributed to the non-uniform rate of stress relaxation, Fig. 5, as the one second m value is about 50% greater than the 10 second value. This suggests a sensitivity of cyclic growth rate to cyclic frequency, with the atypically high rate for high frequency. James' result on the 316 alloy shows a higher growth rate pattern that that of Shahinian. If the Shahinian data is matched, the value of ϵ_G, Fig. 8, is raised into consistency with other alloys. The process zone size d_T appears identical (530 μin.) for each of these alloys, its relatively high value contributory to their high toughness.

12 AND 10% Ni MARAGING STEELS

The extensive data of Barsom, Imhof and Rolfe (34) is modeled in this instance: Fig. 11 for the 12Ni, 5Cr, 3Mo alloy; Fig. 12 for the 10Ni, Cr, Mo, Co. In the extensive 10Ni set, a value of $\epsilon_R = 0.002$ is shown, although an even lower value, say 0.001 would fit as well. For such a hard material, a low value might be expected. This suggests a very low sensitivity to stress ratio, which is, in fact, the observation of Barsom et al on this data which comprises a large range of R values.

The plane strain branch is followed at the top, as would be expected for the relatively thick (1 in.) specimens employed in this high strength material. The difference between thin and thick section branches is not large in the cycled material. Just the opposite is true of the

virgin material where the instability point shifts upward by a factor of about three, in both alloys, into correspondence with the measured plane strain fracture toughness K_{Ic}.

From the 12Ni steel data of Barsom et al, Fig. 11, it is possible to discuss corrosion-fatigue effects; their growth rates in salt water was observed to be quite frequency sensitive. The model result, Eq. 15, allows for a corrosion rate V_S as a multiplicative factor, operating on the same flow variables. For given corrosion rate V_S, the log-log growth rate curves should retain the same shape, being simply displaced upward a distance proportional to the log of the cyclic period Δt. This expectation appears to be realized in this data, Fig. 11. The degree of displacement required to make the fit can be used to estimate V_S. If we approximate $\Delta t \simeq 1/4f$, where f is the cyclic frequency, and use reference values of da/dN the same as discussed for the A533B steel (Sec. 7) then from Eq. 15

$$V_S \simeq \epsilon_G \, f/2\left[\left(\frac{da}{dN}\ \text{CF ref.}\right)-\left(\frac{da}{dN}\ \text{dry ref.}\right)\right]$$

where (da/dN CF ref) is the reference growth rate for the corrosion fatigue match, while (da/dN dry ref.) is that for no environmental effect. Values of V_S so calculated (Table I) are fairly consistent, and as will be evident in a later comparison (Fig. 21), too high for marine environment

AISI4340 9-4-20 and 9-4-25 STEELS

Both fatigue and corrosion fatigue data are available on 4340 steel, Fig. 13. The specimens used for the flow measurements were of Gallagher's stock (35) of a slightly higher tempering temperature than that for Miller's fatigue data (36). Prior experience with tempering

temperatures ranging through this region suggest only a small effect of this difference (16). The match of fatigue data is satisfactory. Again as for the (high strength) maraging steels, only a small R correction, $\epsilon_R \simeq 0.002$, is required. The cyclic curve, traced in from another test on the inset record which records a second cycle fracture, is so rounded that there is little difference between thin and thick section predictions (thus the former not shown). Unlike A533B and stainless steels, this hard alloy cyclicly softens, as expected after Manson (37), so that the fatigue growth is stable well beyond the K_{Ic} level.

Gallagher's stress corrosion cracking velocity data on this alloy has been fitted by an upward translation of the first cycle flow prediction. The growth threshold for this non-coherent-carbide phase steel is not expected to be augmented by a triaxiality factor, as discussed in Sec. (4). The simple fit of the threshold is quite satisfactory, as is that for the K_{Ic} limit. The intermediate velocities fit well except near the threshold where they seem inordinately high and invarient, particularly with the unbuffered salt water. The behavior is more as though the K-proportional ϵ_G should apply. Indeed Sullivan (38) has observed a ratcheting up to and down from this limit in a similar 4340. Further study is needed here. The V_S value emerging this match is noted in Table I.

Only fairly high growth rates, i.e. above 5 μin./cycle are reported for the 9Ni,4Co, 0.20-0.25C steels by Clark (37) and by Crooker (40). The fit is as good as can be expected. Crooker's growth rates typically run somewhat faster than Clark's. The fitting has favored Clark's since it is the more extensive of the data sets.

TITANIUM ALLOYS, 8Al 1Mo 1V and 6Al 4V

For years after World War II, students of the welded cargo ship fracture problem continued to investigate one of the more brittle ship steels produced - the notorious Project E lot. The late Noah Kahn (41) eventually complained to the Ship Structure Committee that the failings of this material were adequately documented so research should turn to the newer tougher materials, however more difficult their assessment. I am afraid a corresponding state of affairs has stemmed from the (timely) discovery by Brown (42) of the extreme stress corrosion cracking sensitivity of an 8-1-1 titanium plate, whose ill-behaved fracturing tendencies are, notwithstanding, to be discussed now.

The cyclic stress strain curves (Fig. 16) show a progressive trend to a slope inversion, a "two-stage" hardening effect, sometimes observed in first cycle properties of titanium alloys. In the fatigue growth prediction (center plot of Fig. 16) this has the effect of stunting and even reversing the crack growth rate prior to the terminal instability rates. When this portion of the T-C derived curve is superimposed on the Meyn (3) fatigue data (lower figure) the prediction appears substantiated, this particularly evident in his more extensive 2 Hz data set. The fitting required a fairly large R correction factor, $\epsilon_R = .006$, for a material of such high relative (to E) strength, for reasons not now understood.

At the very low cyclic frequencies, the corrosion (V_S) induced growth per cycle has increased by a factor of 30 to well above d_T/cycle. It might be expected that the crack would reach into material less affected by the cyclic straining in such a large constant-load growth increment. The

scant data at 1/2 Hz suggests this, where two of the points can be fitted by the first cycle prediction (T), others by the cyclic prediction (T-C) as though the population were bimodal.

Meyn (3) has observed that the corrosion effect in fatigue of this alloy disappears for $\Delta K(=K_{max}$ for R = 0) around the (static) stress corrosion cracking threshold K_{Iscc}. The threshold in this coherent precipitate material should be the first cycle result augmented by a triaxiality factor T.F. = $(1/1-2\nu) \simeq 2.8$ (A corresponding result is observed in the 7075 Al Fig. 18 and 7079, Fig. 19). If the appropriate transposition is applied to the first cycle curve, it does appear to bound the transition region. The fatigue growth rate below the threshold is reasonably well fitted by the predictive curves, although Meyn's vacuum data (not shown) is not, except in his coarse grain results(not shown). The reference growth rate has been based, as in other alloys of this study,on the high frequency room air data.

The values of V_S implied by the corrosion fatigue frequency effect data fitting are seen in Table I to be internally consistent, and also consistent with the value obtained in matching first cycle predictions with Sullivan's (18) stress corrosion cracking velocity (V-K) data. It should be noted here that the same value of ϵ_G was used for first cycle as for reversed cycled predictions, implying that the crack tip strain gradient is not only constant with respect to loading level but unaffected by prior strain history. Use of the K-proportional ϵ_G in this instance would reverse the upward slope of the velocity prediction, and, as already observed by Sullivan (18), fail to fit the fracture data.

The value of V_S for this 8-1-1 titanium in salt water, Table I (Fig. 21), is higher than for any other material of our experience. A number of less active reagents have been tried by Blackburn, Feeney and Beck (43) the two matched in the upper frame of Fig. 16 appear in reasonable agreement with model prediction as to V-K curve shape.

The 6Al 4V titanium alloy results of Crooker (45) and of Clark (39) are displayed in the Fracture-Flow Diagram form in Fig. 17. The growth limit of first cycle ductility corresponds well with K_{Ic}. As in the 8-1-1 alloy, a strain hardening inflection develops, with corresponding growth rate inversion. Clark (39) has favored us with a single data point which suggests this possibility. Crooker's rates rise to infinity in the inflection region, possibly a section yielding effect. The lower tail on Clark's data is believed to be a typical start-up surge, not a true threshold. Early cycles from a low stress fatigue crack could reflect the lower strain hardening rates of the uncycled material, giving the appearance of a temporary surge in growth rate.

ALUMINUM ALLOYS 7075T6, 7079T6 and 5456T321

Aluminum 7075T6 is to practicioners of experimental Fracture Mechanics as Project E was to transition temperature students of old and recently as 8-1-1 to stress corrosion crackers. The long standing propagation data of McEvily and Illg (45), in its Paris ΔK reformulation (47), is nicely fitted by the Fracture-Flow diagram modeling, Fig. 18. The K_{Ic} prediction is slightly higher than usual measured values. A stress corrosion cracking velocity much slower than for 4340 steel or 8-1-1 titanium is indicated by the downward rather than upward shift of the first cycle prediction to fit the data of Hyatt and Speidel (47).

A new result here is the tracking of the predicted curve shape in the "tail-off" in growth rate toward the threshold. In the 7079 T-6, Fig. 19, the lowest velocity point suggests that some excursion down the elastic 1:1 stability line may forestall the zero growth goal. The scatter in the SCC growth rate above the knee of the curve could be a result of a transitional stage from the triaxially inhibited yielding to a fully plastic ligament condition.

Clark's fatigue propagation data on the 7079-T6 seems to definitely favor the plane strain prediction, Fig. 19, as befits his utilization of thick specimens. This is true also in the softer 5456 Alloy, Fig. 20, whereas Crooker's data tends to favor the plane stress prediction in its emergence to infinite growth rate.

DISCUSSION AND CONCLUSIONS

Specific results have been treated in preceding discourse of particular examples. We believe a general concordance of "theory" and experiment has been demonstrated. Its only conspiciously unsatisfactory aspect is the necessity for arbitrary assignment of the gradient strain ϵ_G. It is possible, though not apparent to us, that this results from deficiencies of the simple elastic analogue plasticity model. The general trend in ϵ_G, decreasing with increasing flow strength (UTS) is reasonable. The crack opening displacement varies inversely as the flow strength (YS), so that the transition between its yield strength dependent strains and the yield strength independent plastic strains away from the crack tip should involve a gradient diminished by flow strength. The minus one slope of the log ϵ_G vs log UTS plot suggests an inverse relationship $\epsilon_G \simeq 4$ ksi/UTS.

Some practical results emerging from this study can be listed in conclusion. One of these, quite unexpected, is the fact that the terminal fatigue growth rate instability can be delayed by conditions of constraint, or plane strain, at the crack tip. It is to our knowledge the only fracture strength behavior beneficiary of the thick section. It can be very substantial indeed. Secondly, it appears that the softer materials owe their more substantive fatigue growth threshold levels to a more substantive plastic zone blockage of the strain excursion at the crack tip upon unloading. But much more needs to be learned about the ϵ_R effect, how flow properties are related to it, how it might be measured from COD experiments during cycling. Thirdly, I would remind you of the beneficial effect of triaxiality in displacing upward the K threshold of stress corrosion cracking, apparently a boon to non-ferrous alloys. A fourth conclusion can be drawn from a plot of all reasonably well documented assessments of the surface attack rate against tensile yield strength, Fig. 21. The scale at the right is a rough conversion of these rates to lifetimes of a loaded part so beset. The point is not in the correlation; there is none; that is the point. There is an enormous variability, not a factor of three or six as for typical E-normalized dry fatigue rates but three or six orders of magnitude. It is the why of this enormous variation - surely corrosion induced - that corrosion experts must address their attentions. We would hope the framework which present results provide will be useful in this quest, by relegating some of the behavioral patterns of stress corrosion cracking to the realm of mechanics.

REFERENCES

1. M. A. Hirt and J. W. Fisher, "Fatigue Crack Growth in Welded Beams", Paper prepared under ONR Contract N-00014-68-A-514; NR064-509, Dec. 1971, to be published.

2. P. C. Paris, "Testing for Very Slow Growth of Fatigue Cracks", Closed Loop, MTS Systems Corp., Vol. 2, No. 5, pp. 11-14 (1970).

3. D. A. Meyn, "An Analysis of Frequency and Amplitude Effects on Corrosion Fatigue Crack Propagation on Ti-8Al-1Mo-1V",Met. Trans., Vol. 2, pp. 853-865 (1971).

4. J. D. Sands, "The Kinetics of Subcritical Cracking and Deformation in a High Strength Steel", PhD Thesis, Lehigh University, 1970.

5. J. M. Krafft, "Strain Hardening vs Stress Relaxation Effects on Fatigue Crack Propagation", Report of NRL Progress, July 1971, pp. 1-10.

6. J. G. Williams and C. E. Turner, "The Plastic Instability Viewpoint of Crack Propagation", Appl. Materials Res., Vol. 3, p. 144 (July 1964).

7. D. P. Clausing, "Effect of Plane Strain State on Ductility and Toughness", Int. J. Fracture Mech., Vol. 6, p. 71 (1970).

8. O. Hoffman and G. Sachs, "Theory of Plasticity for Engineers", McGraw-Hill, New York, 1953, Chap. 14.

9. G. Sachs and G. Lubahn, "The Effect of Triaxiality on the Technical Cohesive Strength of Steels", J. Appl. Mech., Vol. 12, p. 211 (1945).

10. J. A. H. Hult and F. A. McClintock, "Elastic-Plastic Strain Distribution around Sharp Notches under Repeated Shear", 9th Int. Congress Appl. Mech., Vol. 8, Univ. Brussels, 1957, p. 51.

11. J. L. Swedlow, M. L. Williams, and W. H. Wang, "Elasto-Plastic Stresses and Strains in Cracked Plates", Proc. 1st Int. Conf. Fracture, Sendai, 1965, Vol. 2, p. 259.

12. J. R.Rice and G. F. Rosengren, "Plane Strain Deformation Near the Crack Tip in a Power Hardening Material", J. Mech. Phys. Solids, Vol. 16, p. 1 (1968).

13. J. W. Hutchinson, "Singular Behaviour at the End of a Tensile Crack in a Hardening Material", J. Mech. Phys. Solids, Vol. 16, p. 13 (1968).

14. H. W. Liu, W. J. Gavigan, and J. S. Ke, "An Engineering Analysis of Ductile Fractures", Int. J. Fracture Mech., Vol. 6, pp. 41-53 (1970).

15. J. H. Underwood and D. P. Kendall, "Measurement of Microscopic Plastic Strain Distributions in the Region of a Crack Tip", Exp. Mech., Vol. 9, p. (1969), or see

J. H. Underwood, J. L. Swedlow, and D. P. Kendall, "Experimental and Analytical Strains in an Edge-Cracked Sheet", Engr. Fracture Mech. Vol. 2, pp. 183-196 (1971).

16. J. M. Krafft and J. H. Mulherin, "Tensile-Ligament Instability and the Growth of Stress-Corrosion Cracks in High-Strength Alloys," ASM Trans. 62:64 (1969).

17. J. M. Krafft and G. R. Irwin, "Crack Velocity Considerations", ASTM Spec. Tech. Publ. 381, p.114 (1965).

18. A. M. Sullivan, "Velocity of Cracks Extending under Stress in an Adverse Environment", Fracture 1969, Proc. 2nd Int. Conf. on Fracture, Brighton, Chapman Hall Ltd., pp 396-405.

19. R. G. Forman, V. E. Kearney, and R. M. Engle, "Numerical Analysis of Crack Propagation in Cyclicly Loaded Structures", ASME Paper Met. 4, 1966.

20. A. Hartman and J. Schijve, "The Effects of Environment and Load Frequency on the Crack Propagation Law for Macro Fatigue Crack Growth in Aluminum Alloys", Eng. Fracture Mech. 1:615, April 1970.

21. J. R. Griffiths, I. L. Mogford, and C. E. Richards, "The Influence of Mean Stress on Fatigue Crack Propagation in a Ferritic Weld Metal", Metal Sci. J., Vol. 5, pp 150-154 (1971).

22. P. C. Paris, W. Weiss, and A. F. Anderson, "On the Threshold for Fatigue Crack Growth", Paper presented at the 5th National Symposium on Fracture Mechanics, U. Illinois, 1 Sept 1971, to be published.

23. P. C. Paris, "The Fracture Mechanics Approach to Fatigue", "Fatigue, an Interdisciplinary Approach", Proc. 10th Sagamore Army Mater. Res. Conf., Syracuse Univ. Press, 1964, pp. 107-132.

24. J. R. Rice, "Mechanics of Crack Tip Deformation and Extension by Fatigue", in Fatigue Crack Propagation, ASTM STP 415:247 (1967).

25. W. Elber, "Fatigue Crack Closure under Cyclic Tension", Engr. Fracture Mech., Vol. 2, pp. 37-46 (1970).

26. J. H. Mulherin and H. Rosenthal, "Influence of Nonequilibrium Second-Phase Particles Formed During Solidification upon the Mechanical Behaviour of an Aluminum Alloy", Met Trans., Vol. 2 pp. 427-432 (1971).

27. J. M. Krafft, "Tests for Fracture Strength, Static Impact", Techniques of Metals Research, Vol. 5, part 2, pp. 1-102, J. Wiley, New York, 1971.

28. W. G. Clark, Jr., "Effect of Temperature and Section Size on Fatigue Crack Growth in Pressure Vessel Steel", J. Materials, Vol. 6, pp. 134-149 (1971).

29. P. C. Paris, R. J. Bucci, E. T. Wessel, W. G. Clark, and T. R. Mager, "An Extensive Study on Low Fatigue Crack Growth Rates in A533 and A508 Steels", Scientific Paper 71-1E7-FMPWR-P7, Westinghouse Res. Corp., 1971.

30. W. O. Shabbits, W. H. Pryle, and E. T. Wessel, "Heavy Section Fracture Toughness Properties of A533 Grade B, Class 1 Steel Plate and Submerged Arc Weldment", Westinghouse Co. Report WC AP 7414, 1969.

31. J. M. Krafft, L. R. Hettche, A. M. Sullivan, and F. J. Loss, "Fracture-Flow Relationship for A533B Pressure Vessel Steel", J. Engr. Industry, Trans, ASME, Vol. 92, p. 330 (1970).

32. L. A. James and E. B. Schwenk, Jr., "Fatigue Crack Propagation Behavior of Type 304 Stainless Steel at Elevated Temperatures", Met. Trans.. Vol. 2, pp. 491-496 (1971). See also

L. A. James, "The Effect of Elevated Temperature Upon the Fatigue-Crack Propagation Behavior of Two Austenitic Stainless Steels, Paper WHAN-SA-105; WADCO Corp., 1971.

33. P. Shahinian, H. E. Watson, H. H. Smith, "Fatigue Crack Growth in Selected Alloys for Reactor Applications", National Symposium on Predictive Testing, Anahiem, Calif., Apr. 1971, ASTM STP forthcoming.

34. J. M. Barsom, E. J. Imhof, and S. T. Rolfe, "Fatigue-Crack Propagation in High Yield-Strength Steels", J. Eng. Fracture Mech., Vol. 2, pp. 319-340 (1971).

35. J. P. Gallagher, "Corrosion Fatigue Crack Growth Rate Behavior above and below K_{Iscc} in Steels", J. Materials,, Vol. 6, pp.941-964 (1971).

36. G. A. Miller, "The Dependence of Fatigue-Crack Growth Rate on the Stress Intensity Factor and the Mechanical Properties of High Strength Steels", Trans. Am. Soc. Metals, Vol. 61, pp. 442-448 (1968).

37. S. S. Manson and M. H. Hirschberg, "Fatigue Behavior in Strain Cycling in the Low-and Intermediate-Cycle Range","Fatigue, an Interdisciplinary Approach", Proc. 10th Sagamore Army Matls. Res. Conf., Syracuse Univ.-Press, 1964, pp. 133-172.

38. A. M. Sullivan, "Stress Corrosion Crack Velocity in 4340 Steel", Forthcoming in Engr. Fracture Mech.

39. R. C. Bates and W. C. Clark, Jr., "Fractography and Fracture Mechanics", ASM Trans. 62:380 (1969).

40. T. W. Crooker, J. A. Cooley, E. A. Lange, and C. N. Freed, "Fatigue Crack Propagation and Plane Strain Fracture Toughness Characteristics of a 9Ni-4Co-0.25C Steel", Trans. Am. Soc. Met., Vol. 61, pp. 568-574 (1968). See also

T. W. Crooker and E. A. Lange, "Corrosion-Fatigue Crack Propagation Studies of Some New High Strength Structural Steels", Trans. ASME, J. Basic Engr., Vol. 91, pp. 570-574 (1969).

41. N. Kahn, Presentation to Ships Structure Committee, Natl. Academy of Sciences, Washington, (around 1960).

42. B. F. Brown, "A New Stress-Corrosion Cracking Test Procedure of High Strength Alloys", ASTM Matl. Res. Std., Vol. 66, p. 129 (1966).

43. M. J. Blackburn, J. A. Feeney, and T. R. Beck, "State-of-the-Art of Stress-Corrosion Cracking of Titanium Alloys", Part 4 of Monograph Review, ARPA Order 878 and NAS7-489, 1970.

44. T. W. Crooker and W. G. Clark, Jr, "Factors Determining the Performance of High Strength Structural Metals", Report of NRL Progress, Mar. 1970, pp. 39-41, (see also Ref. 39).

45. A. J. McEvily and W. Illg, "The Rate of Fatigue Crack Propagation in Two Aluminum Alloys," NASA TN 4344, 1958 .

46. P. Paris and F. Erdogan, "A Critical Analysis of Crack Propagation Laws," ASME Trans. 85D:528 (1963).

47. M. V. Hyatt and M. O. Speidel, "State-of-the-Art of Stress-Corrosion Cracking of High-Strength Aluminum Alloys", Part 6 of Monograph Review, ARPA Order 878, 1970.

TABLE 1
COMPOSITION, FLOW PROPERTIES, FRACTURE BEHAVIORS OF VARIOUS ALLOYS

		STEEL	STAINLESS		MARAGE			Q&T			TITANIUMS				ALUMINUMS		
Material		A533B	316 SS	304SS	12Ni	10Ni	4340	9-4-20	9-4-25		8-1-1	6-4			7075	7079	5456
		Fe+	Fe+	Fe+	Fe+	Fe+	Fe+	Fe+	Fe+		Ti+	Ti+			Al+	Al+	Al+
Composition Wt. %	C	0.19	0.060	0.053	0.02	0.123	0.40	(0.20)	0.25	Al	7.4	6.3	Si		0.3	0.14	
	Mn	1.34	1.72	0.87	0.06	0.17	0.72	(0.30)	0.28	Mo	1.16		Fe		0.4	0.29	
	Si	0.25	0.40	0.49	0.06	0.04	0.28	(0.01)	0.01	V	0.86	4.1	Cu	1.5	0.6	0.08	
	Al				0.35	0.02				Fe	0.14	0.13	Mn		0.2	0.68	
	Ni	0.53	13.3	9.5	18.2	10.11	1.70	(9.0)	8.31	C	0.08	0.023	Mg	2.5	0.3	5.17	
	Cr	0.13	17.3	18.3	4.9	2.06	0.80	(0.75)	0.40	O	0.09	0.17	Cr	0.3	0.2	0.08	
	Mo	0.42	2.33	0.18	2.9	1.06	0.24	(1.0)	0.48	N	0.004	0.014	Zn	5.5	4.3	0.03	
	B	0.017	0.012	0.010	0.009	0.006	0.01	(0.01)	0.008	H		0.004	Ti		0.1	0.03	
	P	0.011	0.007	0.019	0.0061	0.009	0.012	(0.01)	0.006								
	Cu	0.16	0.065	0.21	0.35												
	V							(0.10)	0.11								
	Co					8.00			3.78								
Heat Treat		Q&T	An	An	Ag Q	Ag Q	Q&T	Q&T	Q&T		An	An			T-6	T-6	H-321
Flow Properties																	
E(10^3 ksi)		29	28	27	27.9	28.7	30	28.6	28.6		17	16.5			10.4	10.4	10.4
σ_0 (10^3 ksi)		60	44	44	43	52	55	40	46		26.5	27			16	16.0	16
$\nu = E/2\sigma_0$		0.24	0.32	0.31	0.32	0.28	0.27	0.36	0.31		0.32	0.31			0.32	0.32	0.32
TF=1/1-2ν		NA	NA	NA	NA	NA	NA	NA	NA		2.8	2.6			2.8	2.8	2.8
TYS (ksi)		61	40	35	185	180	210	180	178		135	116			75	75	34
UTS (ksi)		87	(95)	(90)	200	210	260	200	196		148	126			89	87	48
ϵ_c B=0		0.16	>0.4	>0.5	0.020	0.042	0.035	0.07	0.07		0.11	0.07			0.11	0.10	0.12
ϵ_c B=1/2		(0.17)	ND	ND	0.090	0.085	0.04	0.11	0.12		0.13	0.10			0.12	0.13	>0.15
T-C UTS ksi		71	120	140	190	200	231	195	187		142	120			91	91	51
T-C ϵ_c,B=0		0.072	0.08	0.10	0.07	0.08	0.045	0.09	0.09		0.10	0.10			0.09	0.08	.06
T-C ϵ_c,B=1/2		0.087	0.17		0.09	ND	0.050	0.11	0.12		0.11	ND			0.10	0.10	09
$\dot{\epsilon}$ 1 sec.		0.0087	0.0161	0.0161	0.0095	0.0089	0.0070	0.0099	0.0100		0.0118	.0138			0.0138	0.0157	0.0081
$\dot{\epsilon}$ 10 sec.		"	0.0105	0.0105	"	0.0066	"	0.0085	0.0083		0.0105	"			0.0129	0.0115	"

Fracture Behaviors Specimen Type		CTS	NCB	CTS-SEN	CTS	CTS	CNS SEN	CNB/CTS		CNS SEN	CNB CTS	CNS	CTS	CTS CNB
Approx.Thick.(in)		0.2,1,2,3,4	0.5	0.5	1.0	1.0	0.15 0.5	0.5/1.0		0.5	0.5/1.0		1.0	0.5/1.0
Crack Direction		ND	LT-TL	LT-TL	ND	ND	----	TL-LT	TL-LT					
Min/Max Stress,R		0-0.8	0-0.05	0.050	0.09	0.1-0.7	0	0	0	0	0	0	0	0
ϵ_{R0}		0.0066	0.009	0.008	ND	(0.002)	(0.002)	(0.002)	(0.002)	0.006	ND	0.002	(0.002)	(0.005)
ϵ_G (1 sec.)		0.062	0.014	0.030	0.243	0.0254	0.0094	0.0265	0.0211	0.0262	0.0495	0.0534	0.0536	0.0694
ϵ_G (10 sec.)		"	0.009	0.020	"	0.0189	"	0.0228	0.0175	0.0233	"	0.0516	0.0392	"
d_T (u in.)		4.8	13.4	13.4	26.0	10.9	10.5	8.2	4.0	7.3	19.9	4.0	3.1	5.3
K_{Ic} meas.		(200)	ND	ND	215	210	65	165	150	87	110	32	27	ND
K_{Ic} pred.		210	>600	>800	200	190	70	140	125	96	110	45	35	>55
Environment		Air	Air	Air	S	Air	S	Air	Air	S	Air	F	F	Air
Freq(HZ)/V_g(in/sec)		Var/ND	Var/ND	Var/ND	10/-- 1/3.6^{-6} 0.1/1.1^{-6}	Var/ND	0/1.47^{-8}	Var/ND	Var/ND	0/1.37^{-8} 10/1.6^{-8} 2/1.9^{-8} 1/2-1.2^{-8} 0/1.2^{-8}(C) 0/1.2^{-7}(CW)	Var	0/1.37^{-9}	0/1.86^{-8}	ND

Var = Varied
ND = Not Determined or Not Available
NA = Not Applicable
( ) = Estimated Value

Environments R. T. Air except
S = Salt Water
F = Fresh Water
C = C H_2Cl_2
CW = C $H_2Cl_2H_2O$ Sat.

Heat treatment
An = Anneal
Au = Austenitise
Ag = Age
N = Normalise
Q = Quench

CTS Compact Tension
SENT Single Edge Notch Tension
CNB Cantilever Notch Bend
CNS Center Notched Sheet

Cracking Direction
L - Longitudinal
T(Width) Transverse
S Short Transverse
1st letter - Crack plane normal
2nd letter - Crack direction

Exponent designates that power of 10

CREEP - GROWTH MODEL

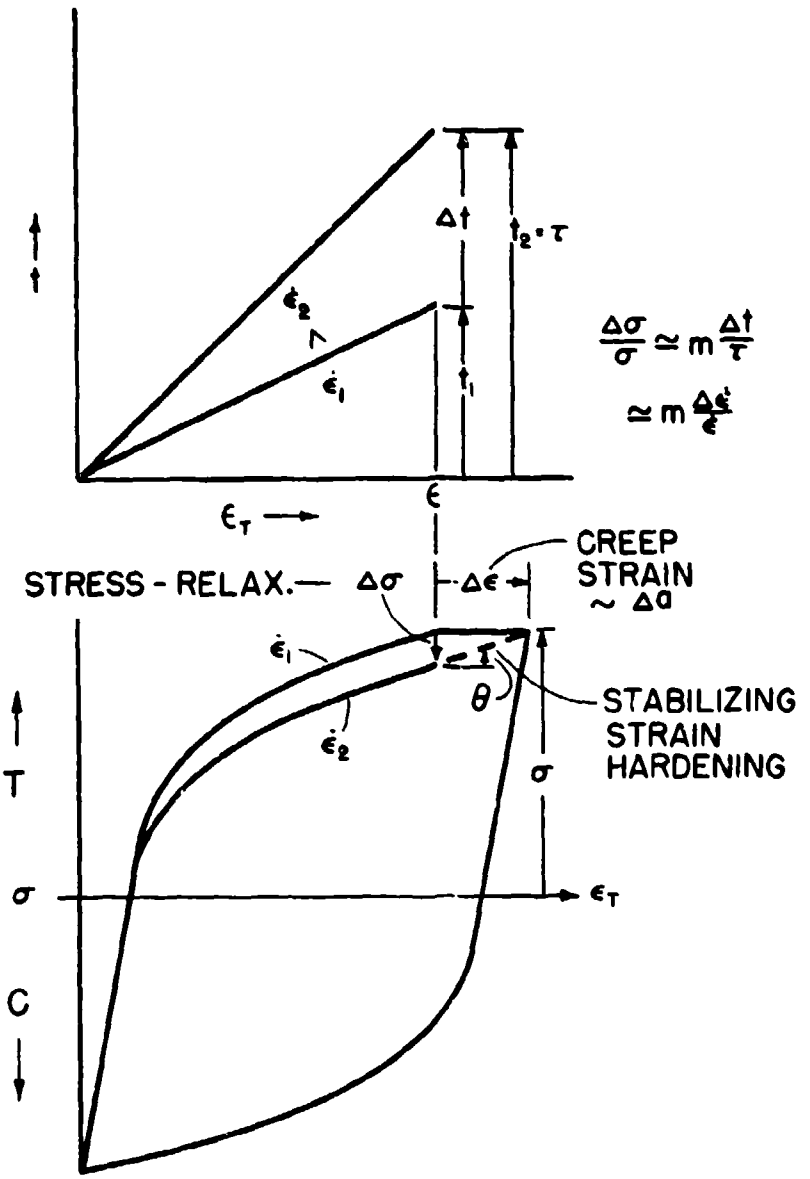

Fig. 1 - Stress relaxation $\Delta\sigma$ in time Δt (upper diagram) is related to the strain rate sensitivity m, and (below) is equilibrated by strain hardening $\theta\Delta\epsilon$ due to crack growth Δa.

CRACK PLASTICITY MODEL

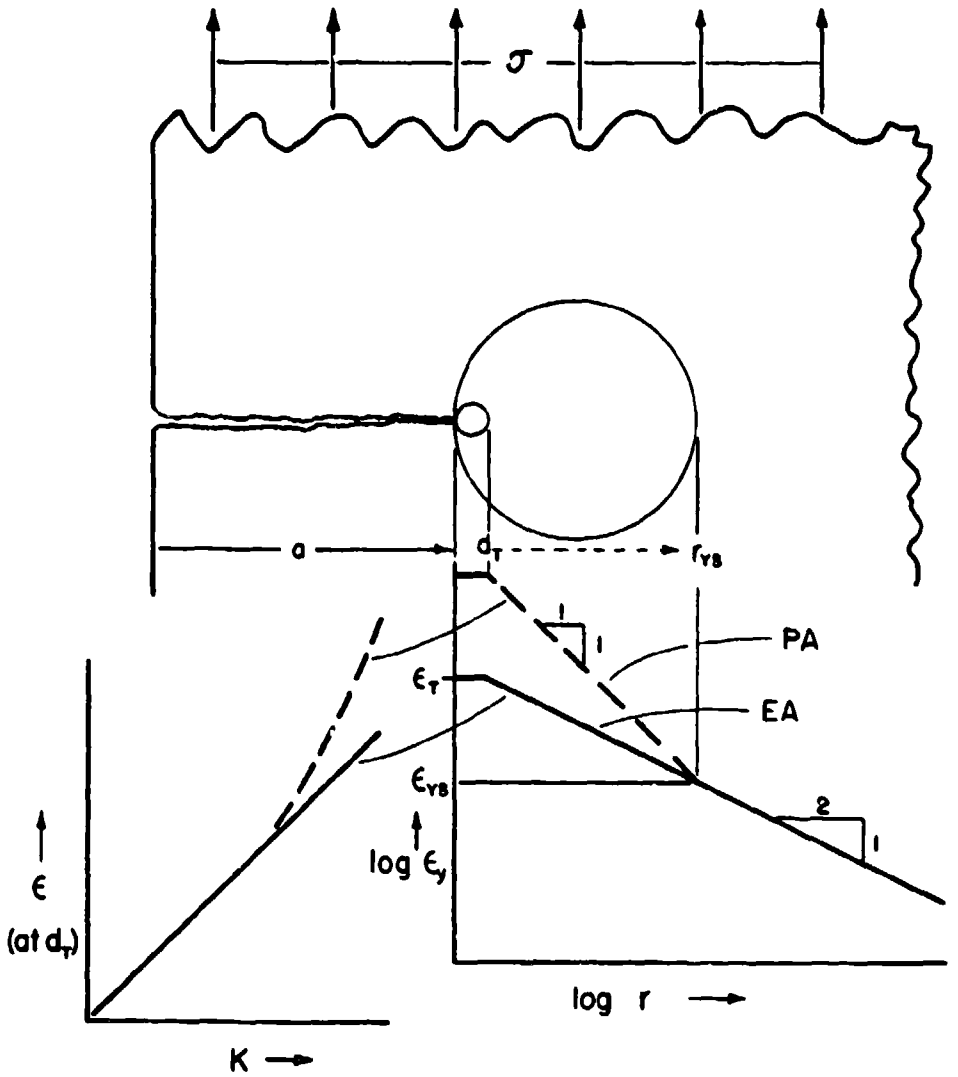

$$K \sim \sigma\sqrt{a} \qquad \epsilon \simeq K/E\sqrt{2\pi r}$$

Fig. 2 - Crack tip d_T - size ligaments undergo plastic strain ϵ when an elastic stress σ is applied because strain field singularity (lower right) concentrates strain. In the elastic analogue model EA, ϵ is proportional to the stress intensity factor K; plasticity models PA predict a larger value.

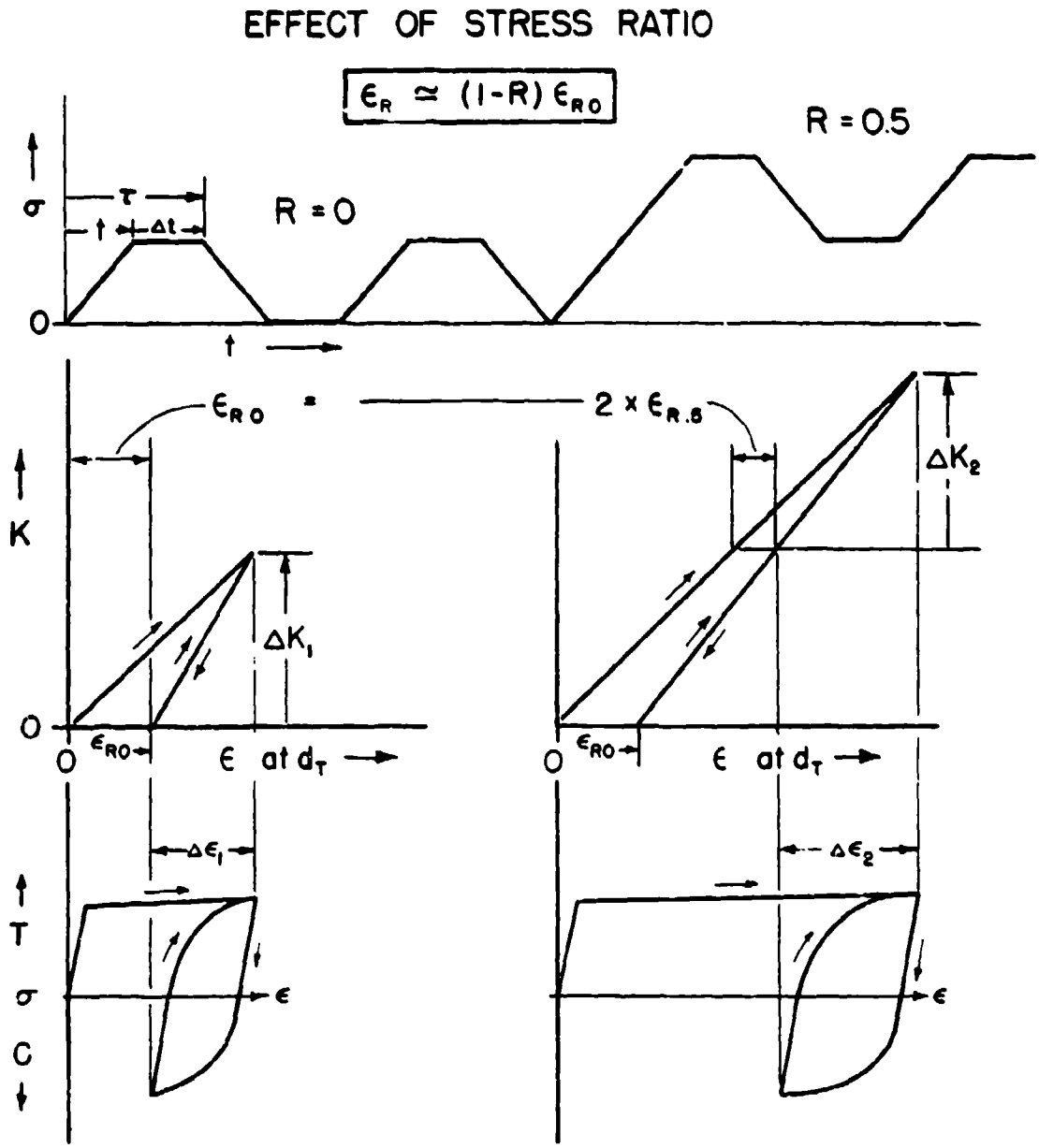

Fig. 3 - Loading, then unloading the crack extends, then compresses the d_T-ligaments. However full compression is blocked by prior tensile distortion, to a degree ϵ_R less for a high stress ratio R than for low.

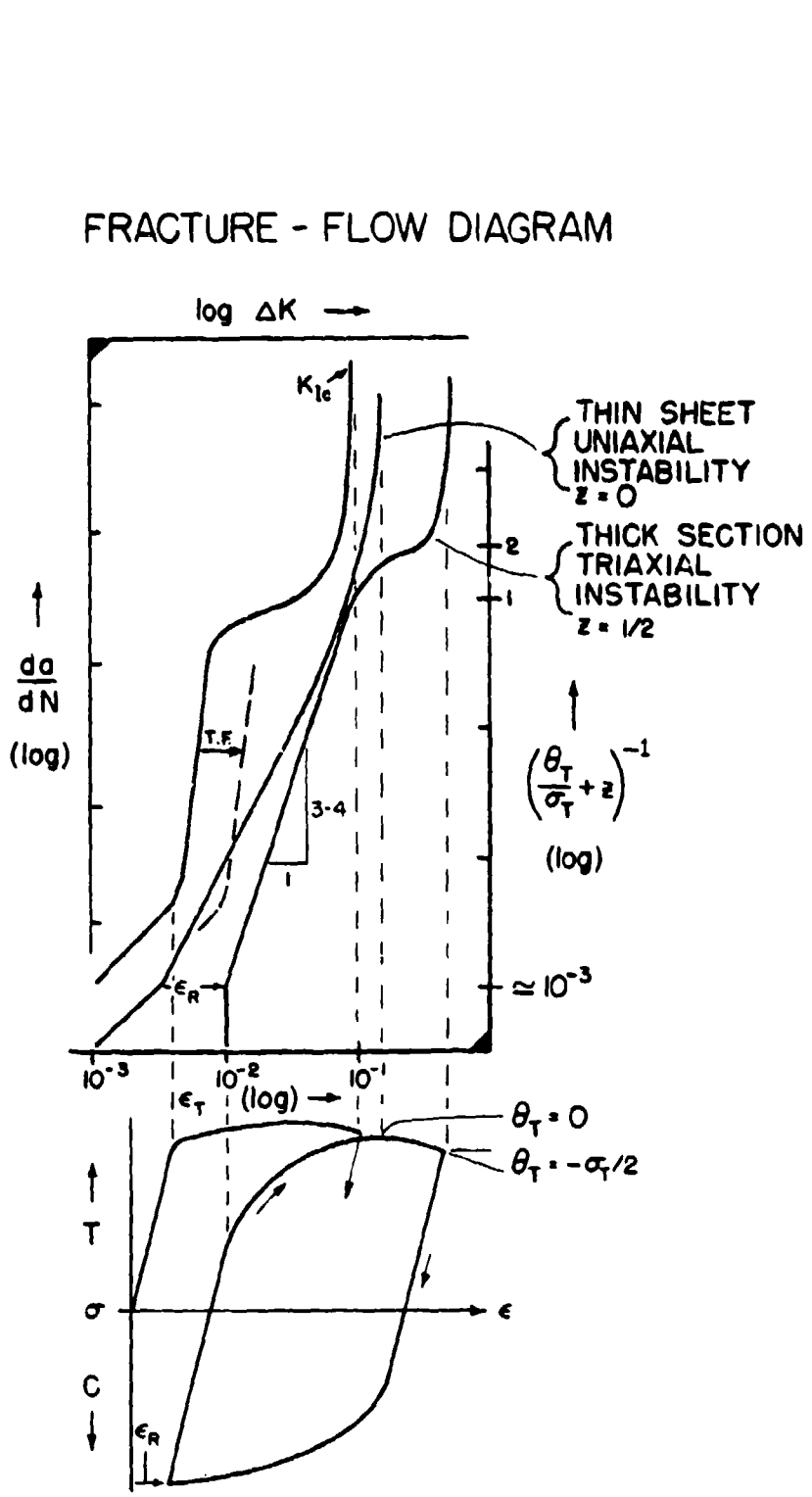

Fig. 4 - Fracure data can be compared to predictions from Flow data by appropriate re-plotting of the stress-strain curves, and allowances for yielding constraint TF and reclosure blockage ϵ_R.

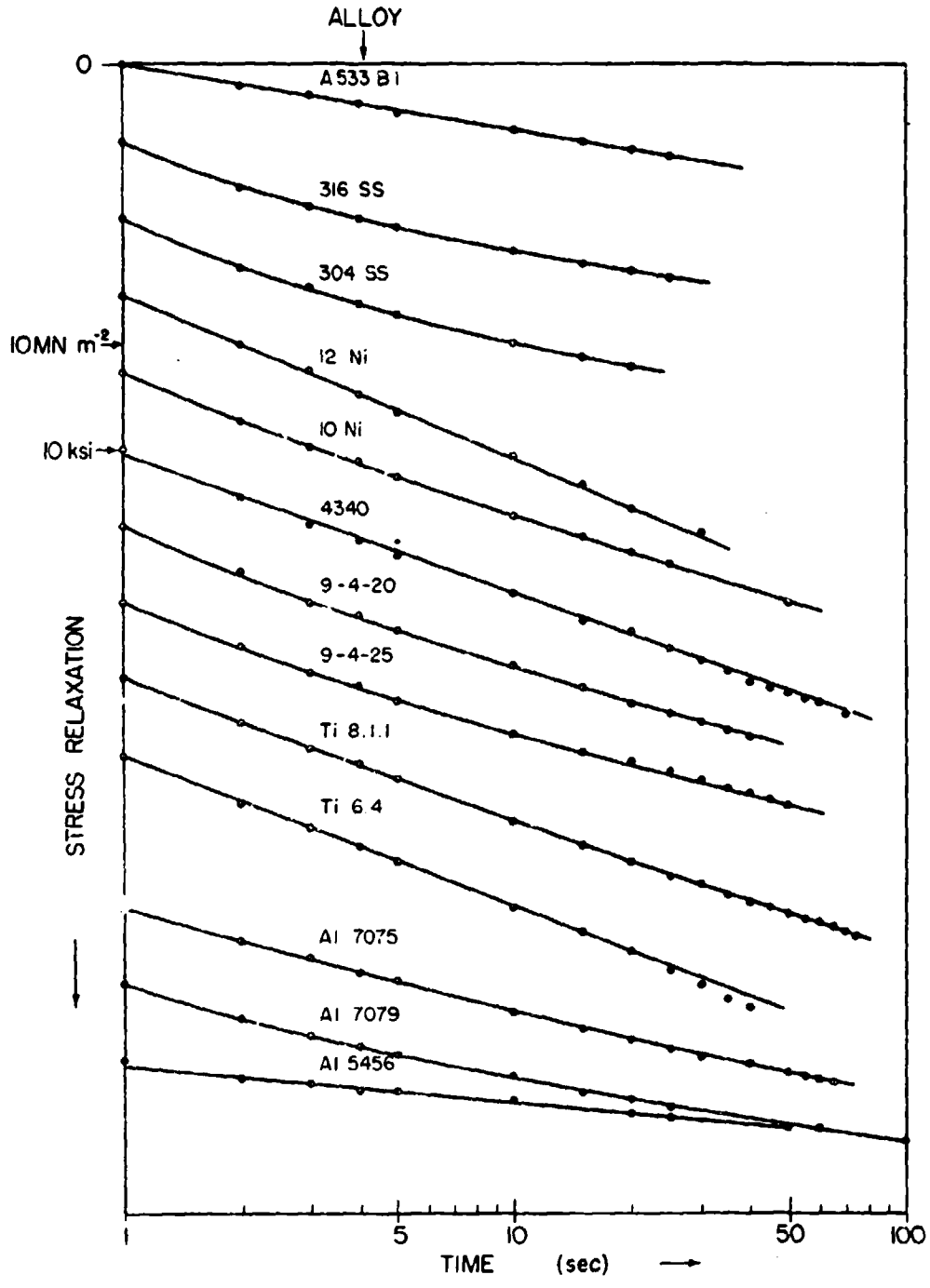

Fig. 5 - Stress relaxation vs log time after sudden arrest of the (hard) testing machine allows assessment of the strain rate sensitivity n for the various alloys.

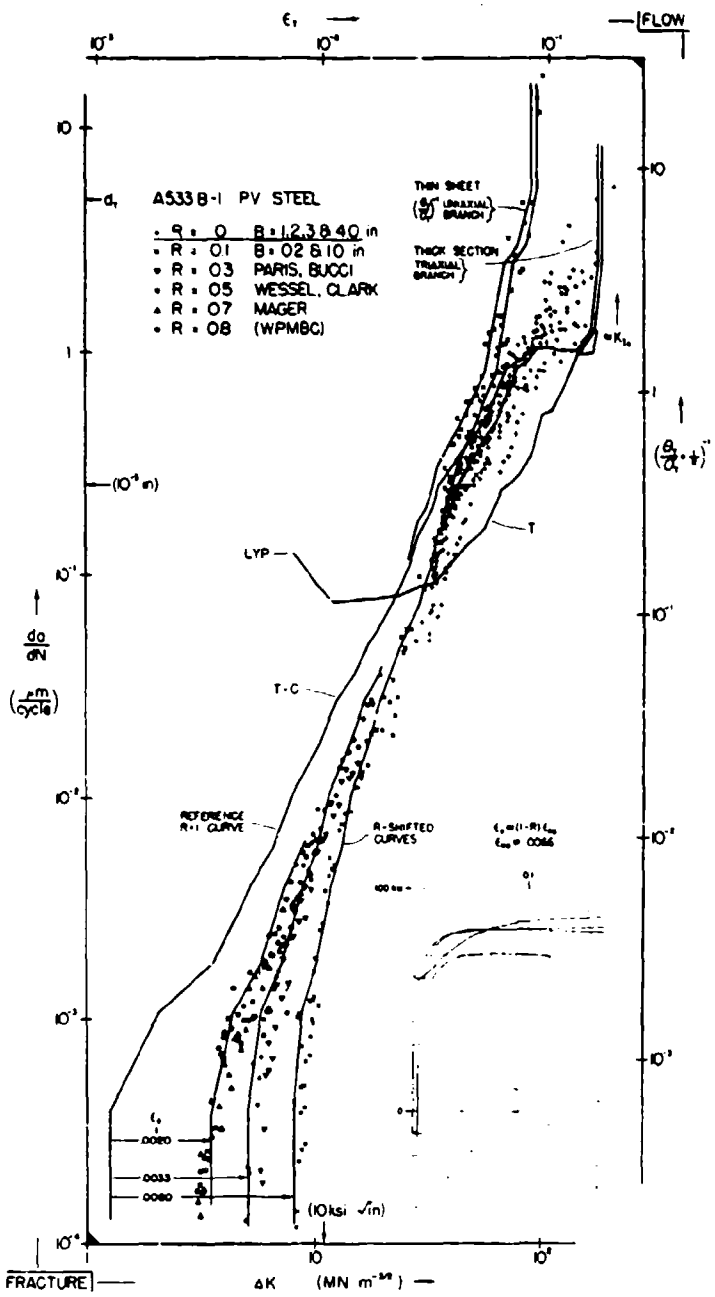

Fig. 6 - The extensive "WPMBC" data on A533B-1 steel is matched to cyclic tension curve (lower right) predictions. The ϵ_R correction shifts the reference curve into agreement with the R-effect at low growth rates. At high rates, the triaxial instability branch fits the thick section fatigue data.

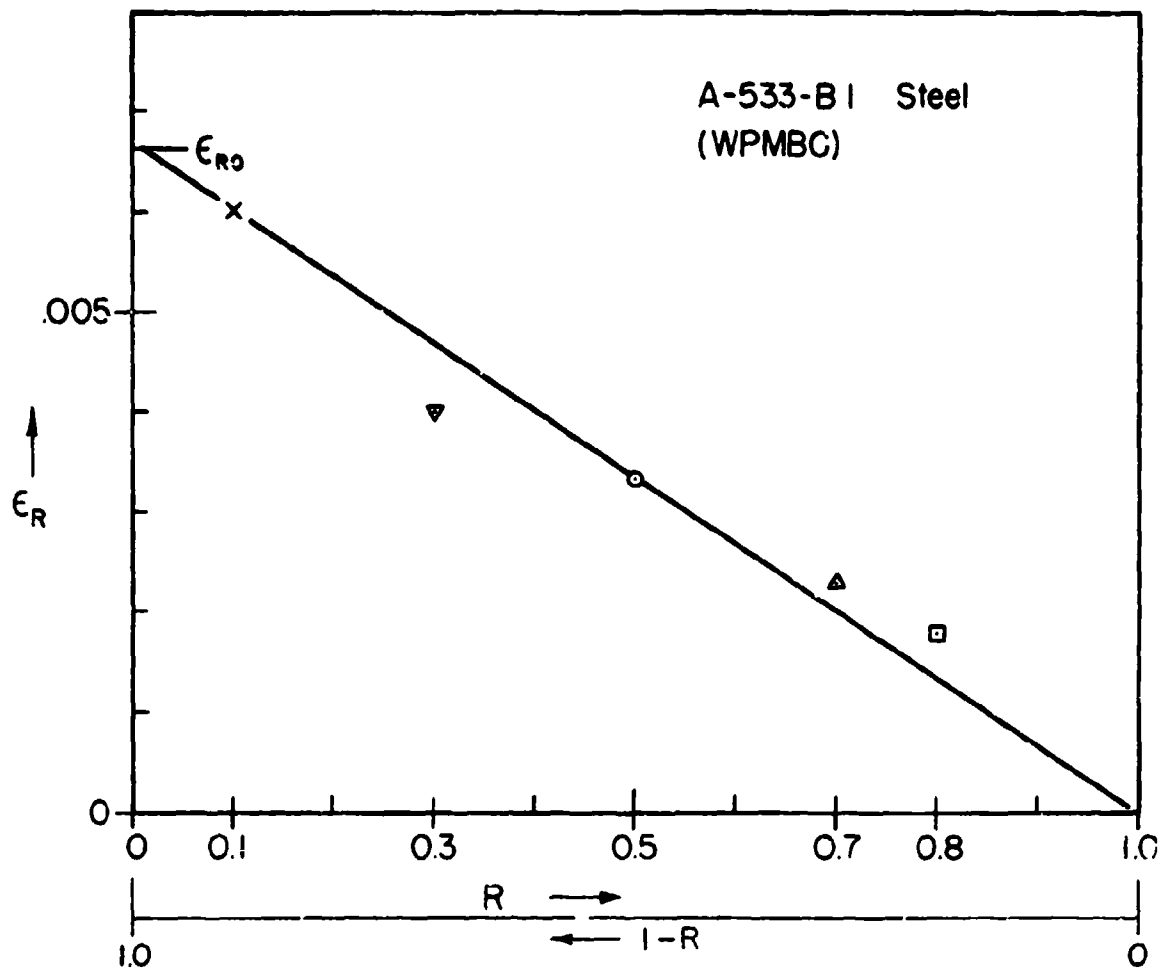

Fig. 7 - The ϵ_R shifts needed to match the A533B-1 data (Fig. 6) conform to the simple model (Fig. 3) trend.

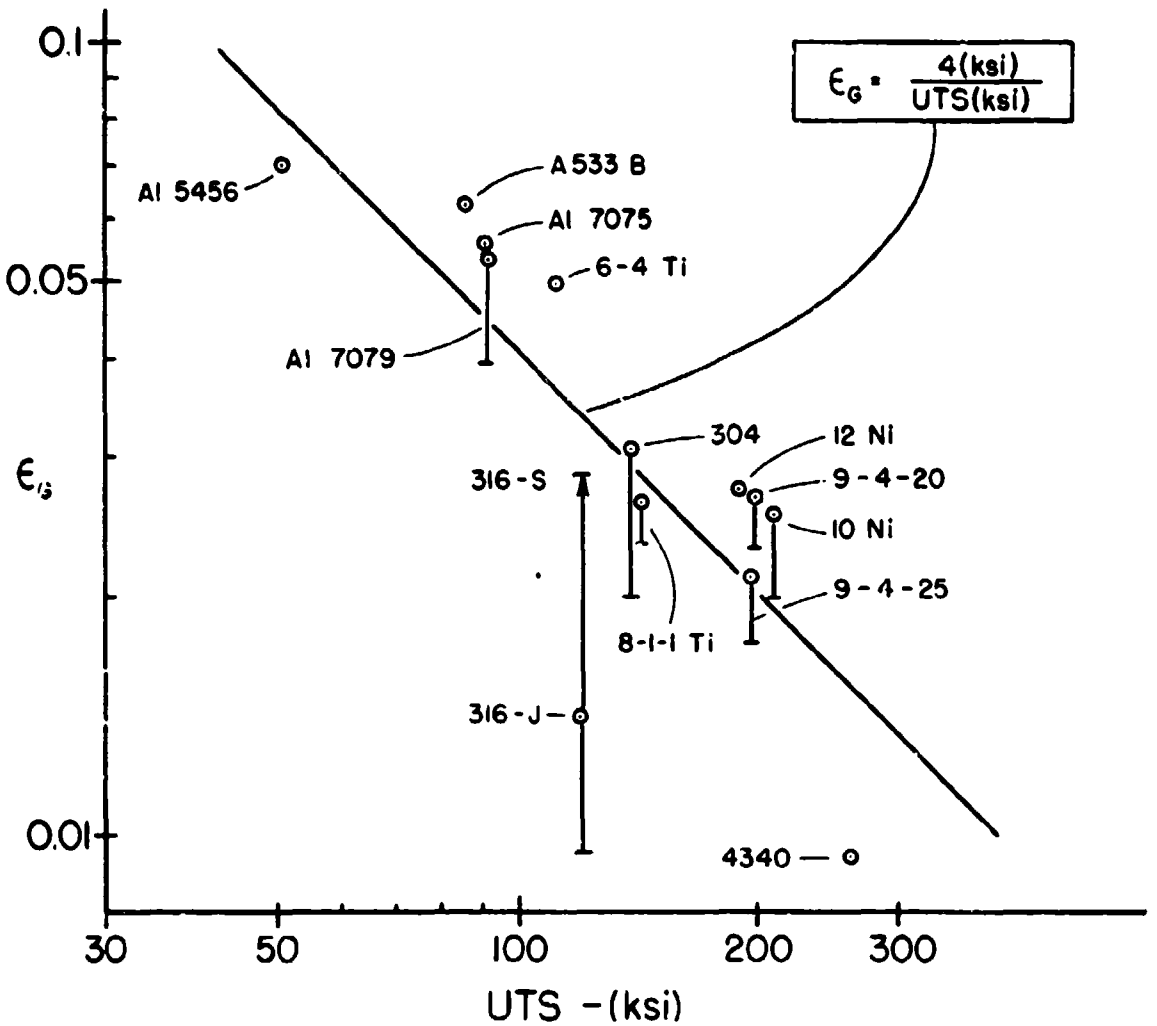

Fig. 8 - Values of the "gradient" strain ϵ_G tend to decrease, inversely, with tensile strength UTS. The lower bars are calculated with 10 sec m values; upper point with 1 sec. Shahinian's stainless steel data 316-S would follow this trend better than James data 316-J which was matched (Fig. 9).

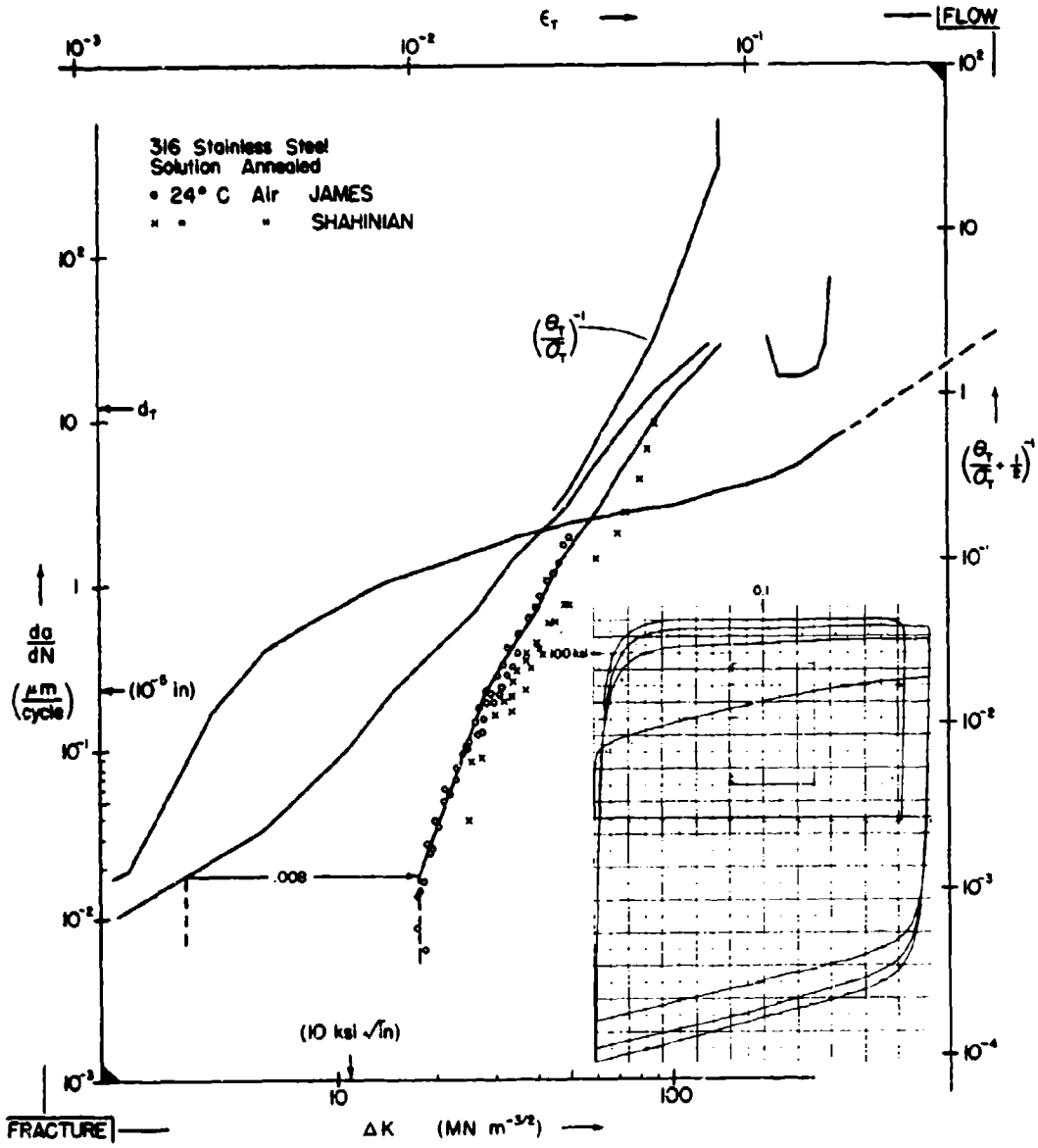

Fig. 9 - Fracture-Flow matching of solution-annealed 316 stainless steel requires a relatively high R effect correction ϵ_R = 0.008, but this is expected for such, soft, cyclicly hardening, material.

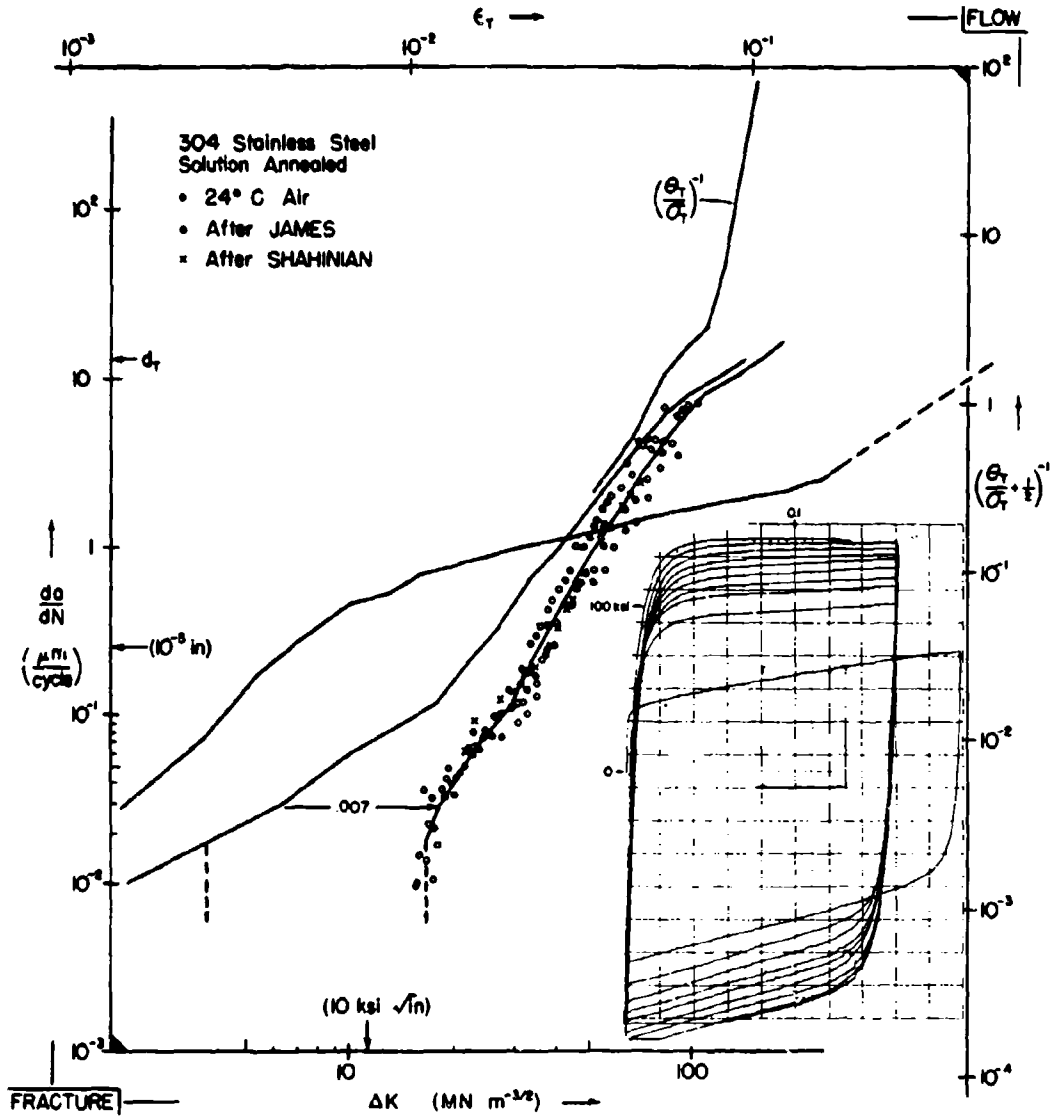

Fig. 10 - For annealed 304 stainless steel, the first cycle tensile instability strain ϵ_c is off scale, indicating, as in 316, an unmeasurably large value of K_{Ic}, yet with cyclic hardening fatigue propagation is normal.

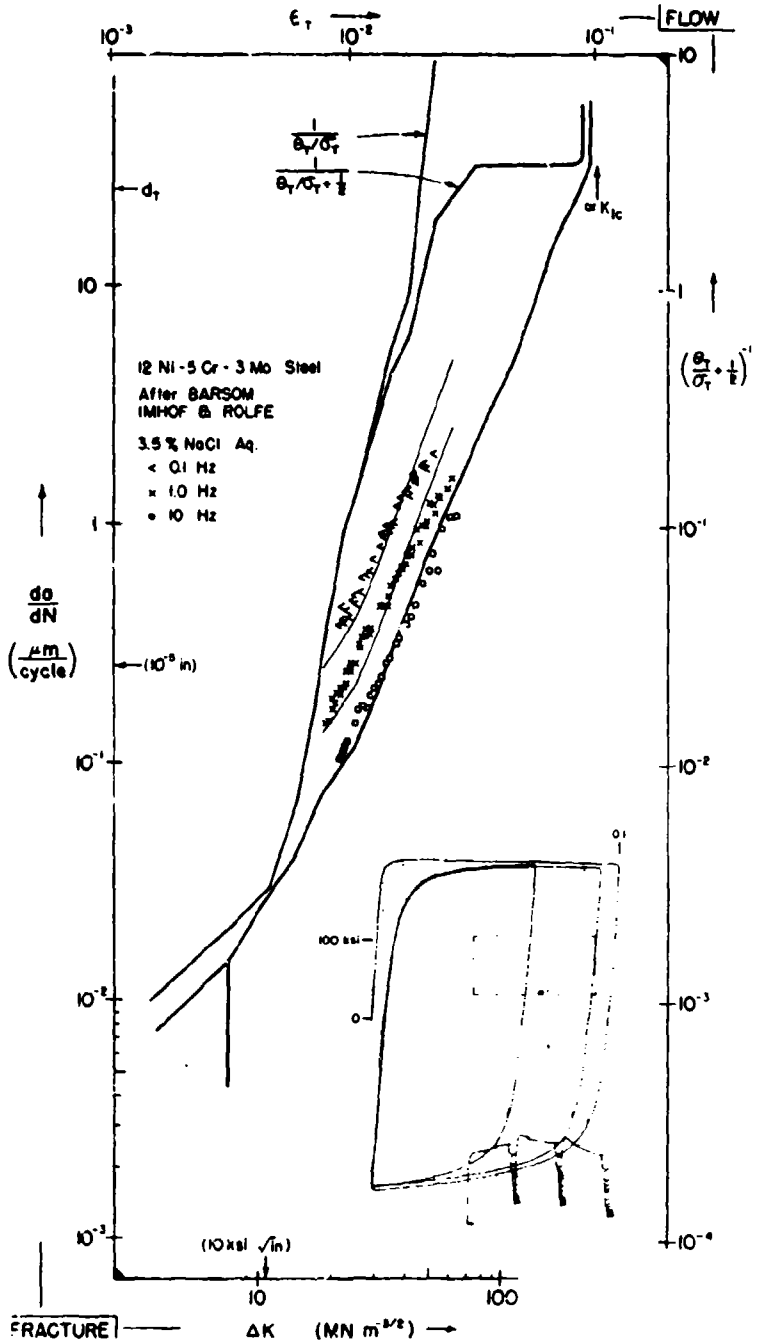

Fig. 11 - Barsom's longer dwell times of lower cyclic frequency of 12Ni steel in salt water exhibited a marked increase in crack growth rate, interpreted as a high V_S - corrosion rate (Table I and Fig. 21). Typical stress relaxation profile at 10X stress gain, are shown in the test record inset.

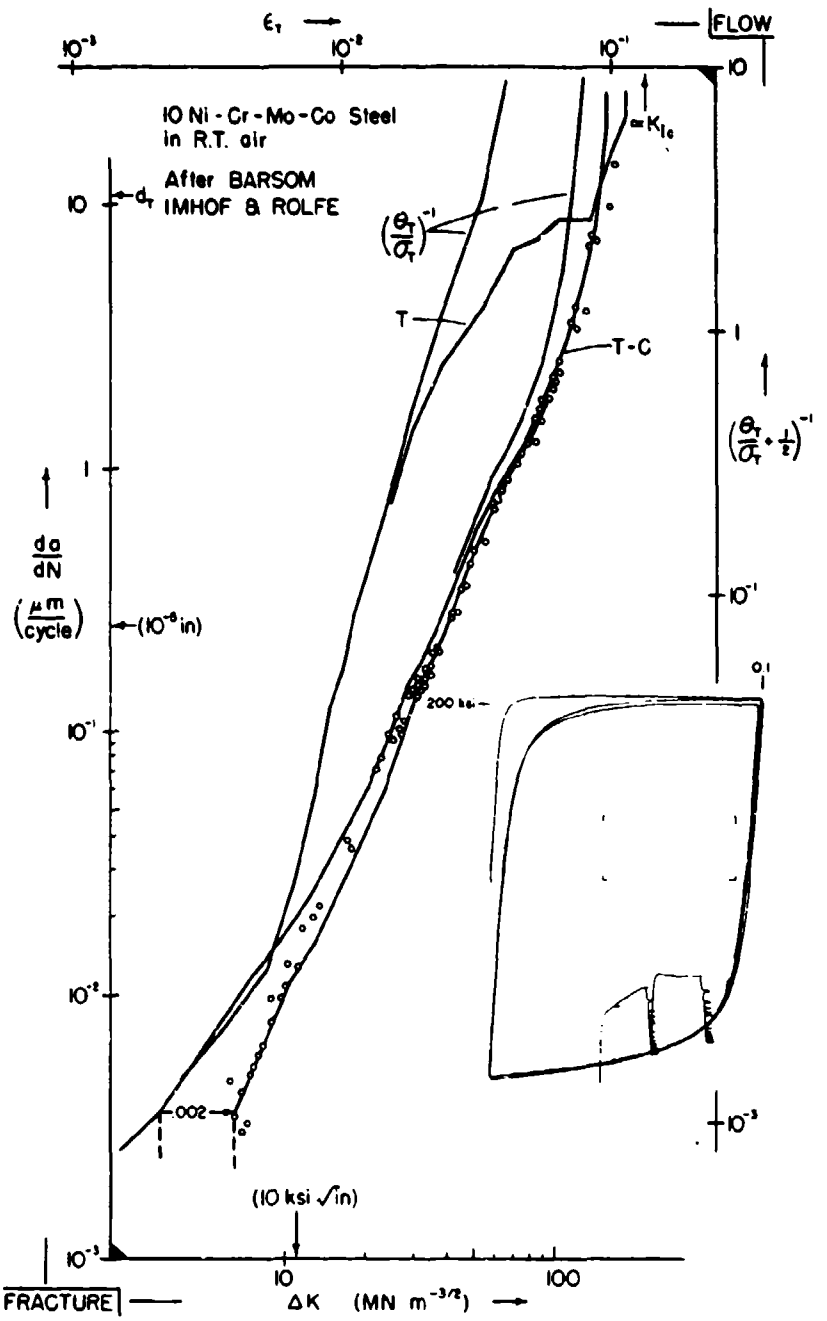

Fig. 12 - The triaxial instability strain of the 10Ni steel, like the 12Ni of Fig. 11, is in agreement with the K_{Ic} value, and far larger than the uniaxial maximum load point.

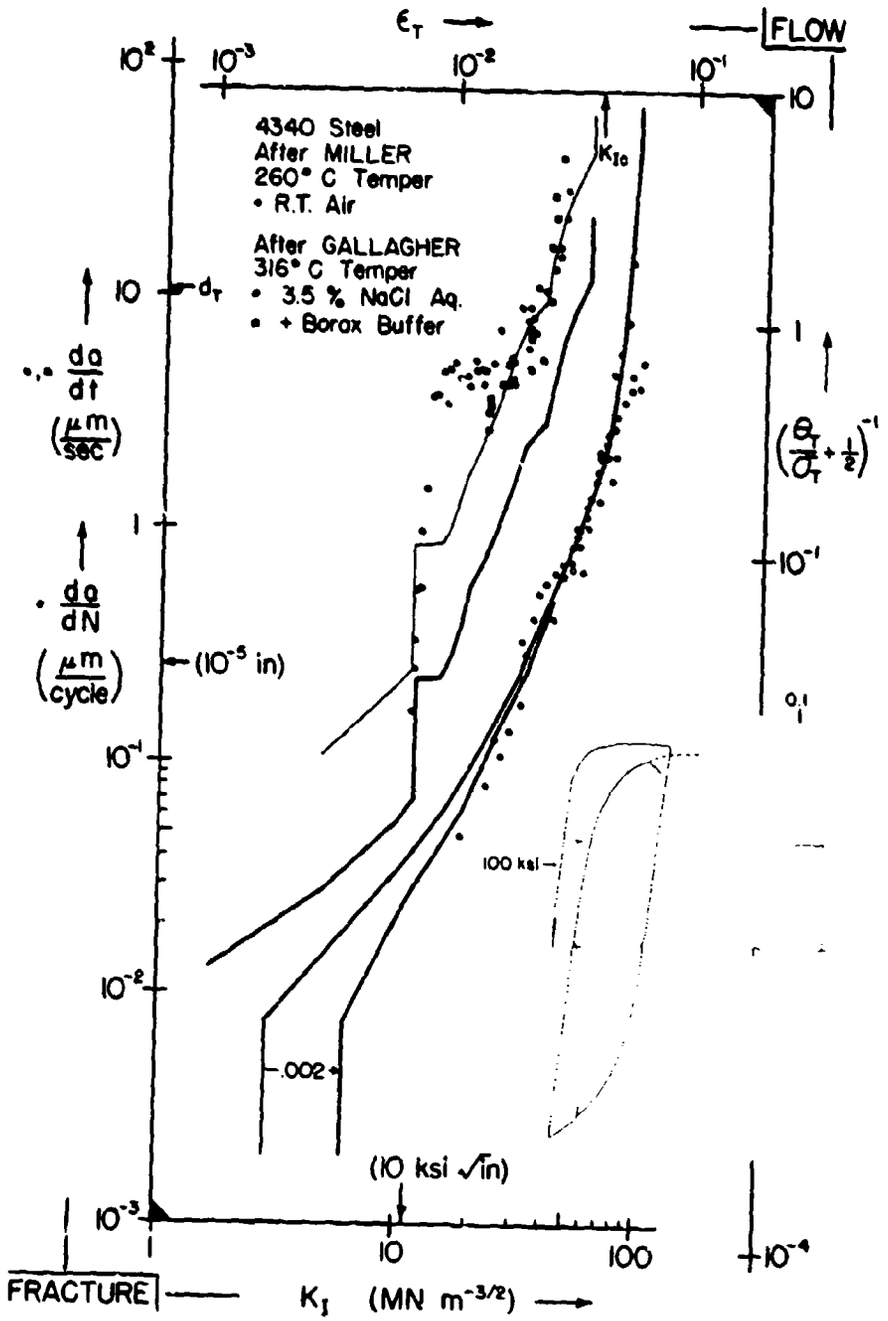

Fig. 13 - The fatigue propagation rate of 4340 steel is fitted by cyclic flow prediction, and stress corrosion cracking by the first tension excursion, The upward shift in matching indicative of a severe environmental sensitivity, high V_S (Fig. 21) in salt water.

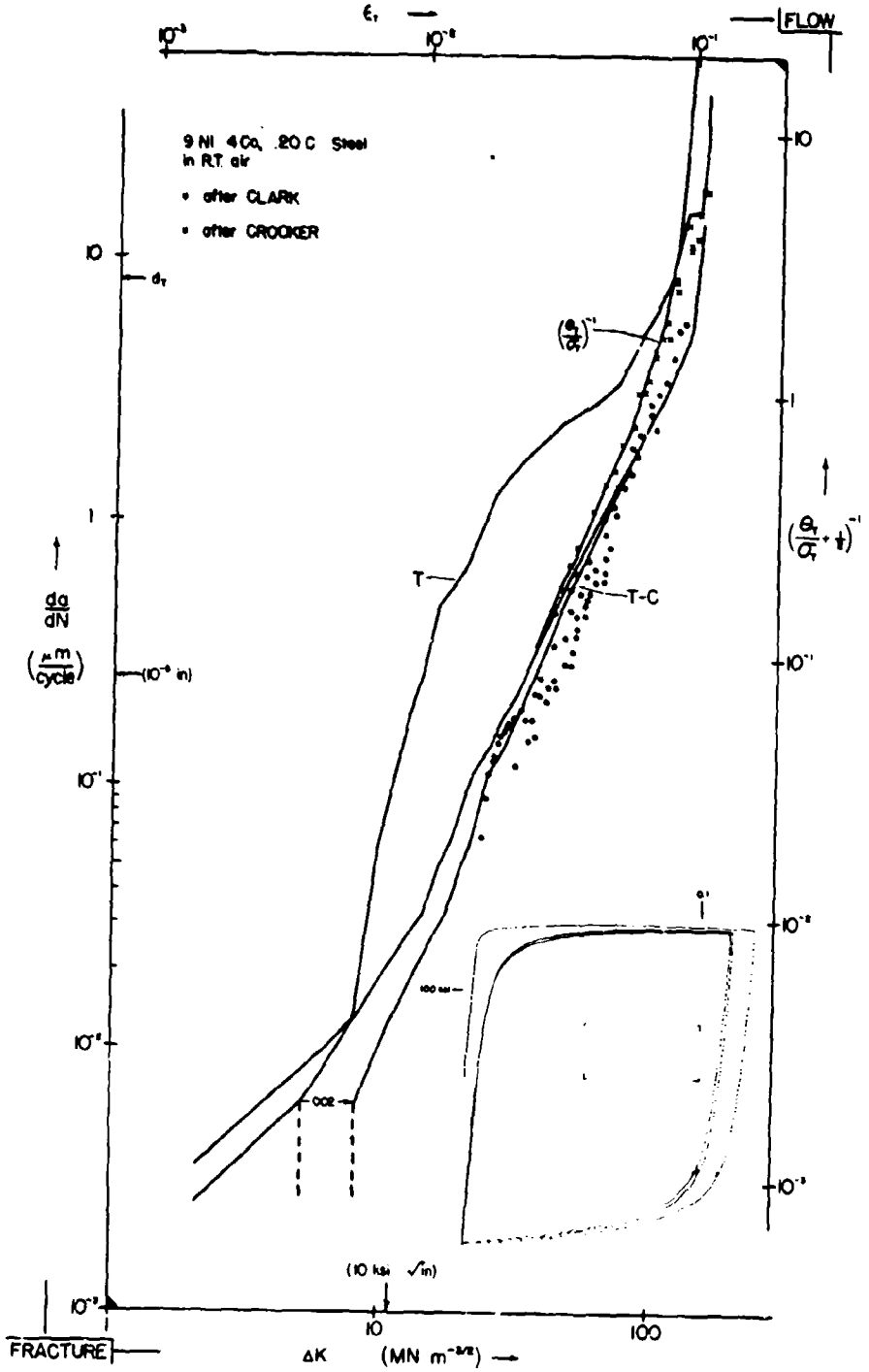

Fig. 14 - Fracture-Flow diagram for 9Ni, 4Co, 0.20C steel.

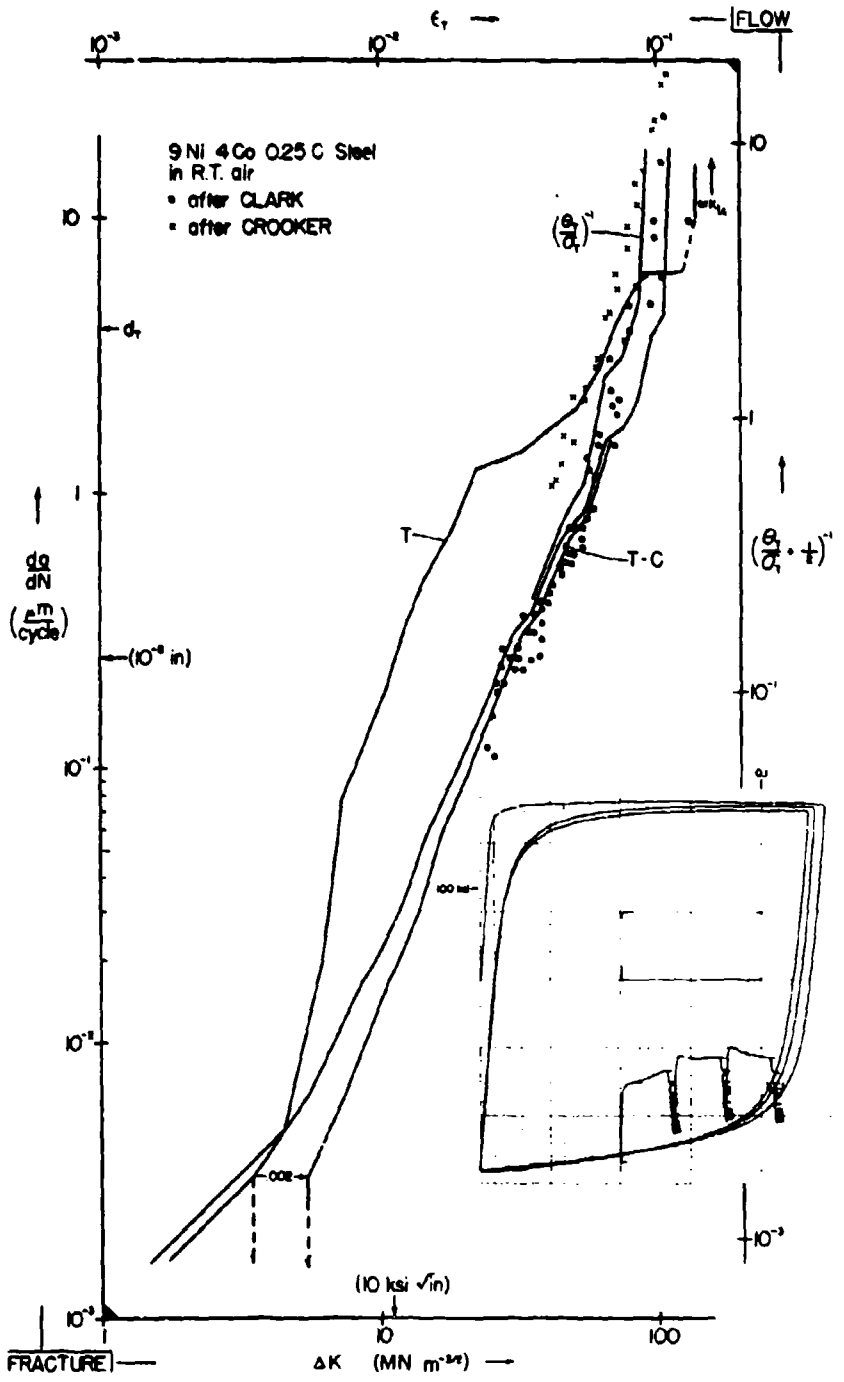

Fig. 15 - Fracture-Flow diagram for 9Ni, 4Co, 0.25C steel.

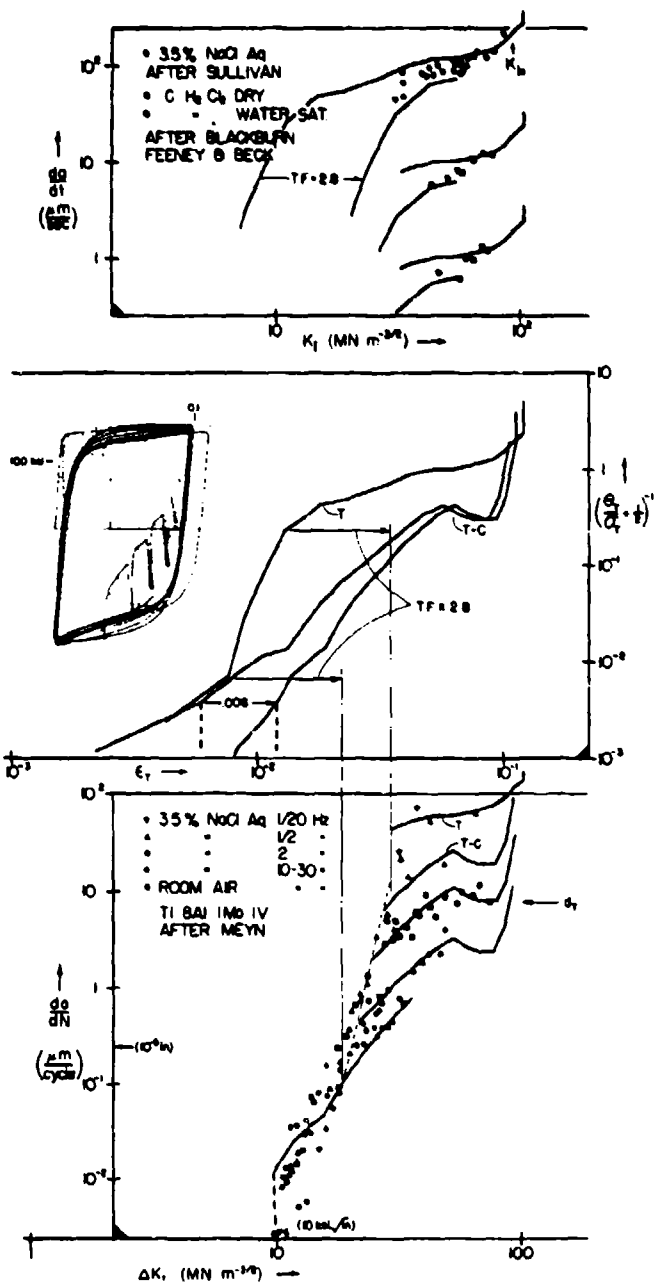

Fig. 16 - The two stage hardening effect in 8-1-1 titanium (center inset) gives an inflection in growth rate (center plot) reflected in Meyn's fatigue data (lower plot). His growth increase with cycle duration yields a V_S value consistent with that for Sullivan's stress corrosion cracking velocity (upper plot). The Blackburn et al data is also matched to first cycle flow prediction with reduced V_S for CH_2Cl_2 environment.

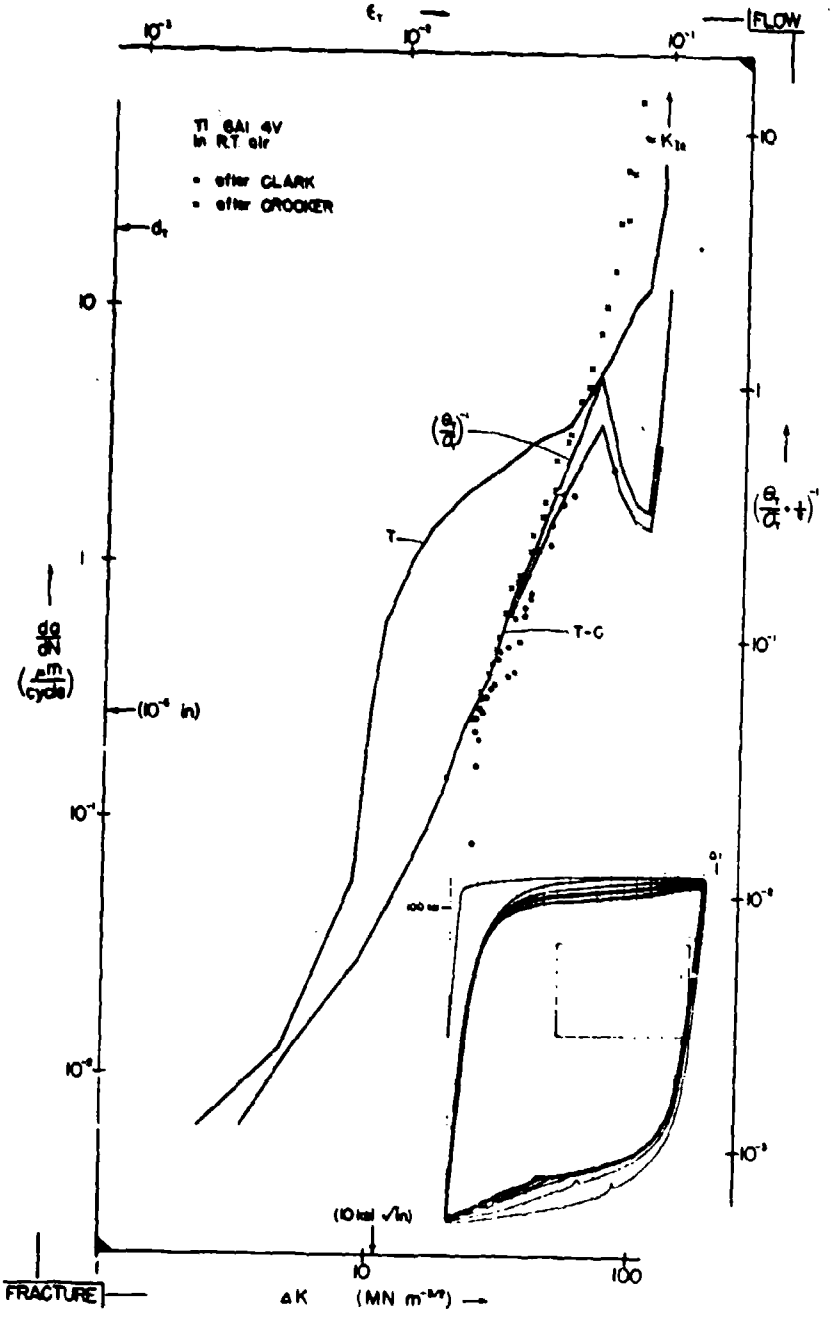

Fig. 17 - Fracture-Flow diagram for 6 Al 4V titanium.

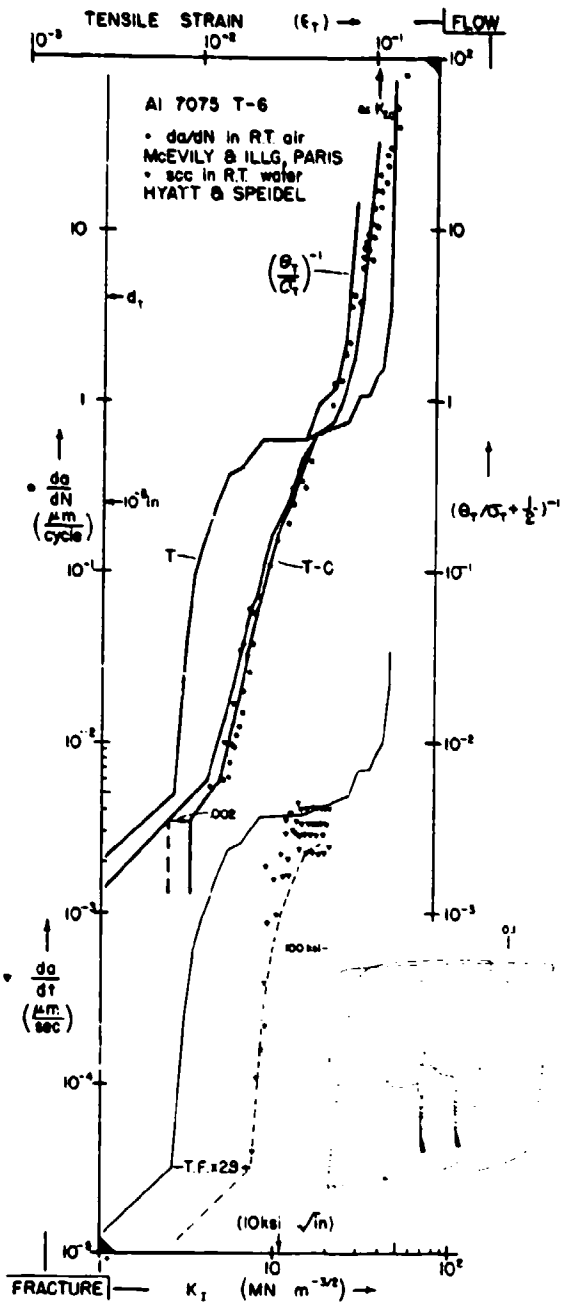

Fig. 18 - The Fracture-Flow diagram match for 7075-T6 aluminum shows agreement with the stress corrosion velocity results of Hyatt and Speidel, the downward translation of first cycle prediction indicative of a slow (V_S) corrosion effect (Fig. 21).

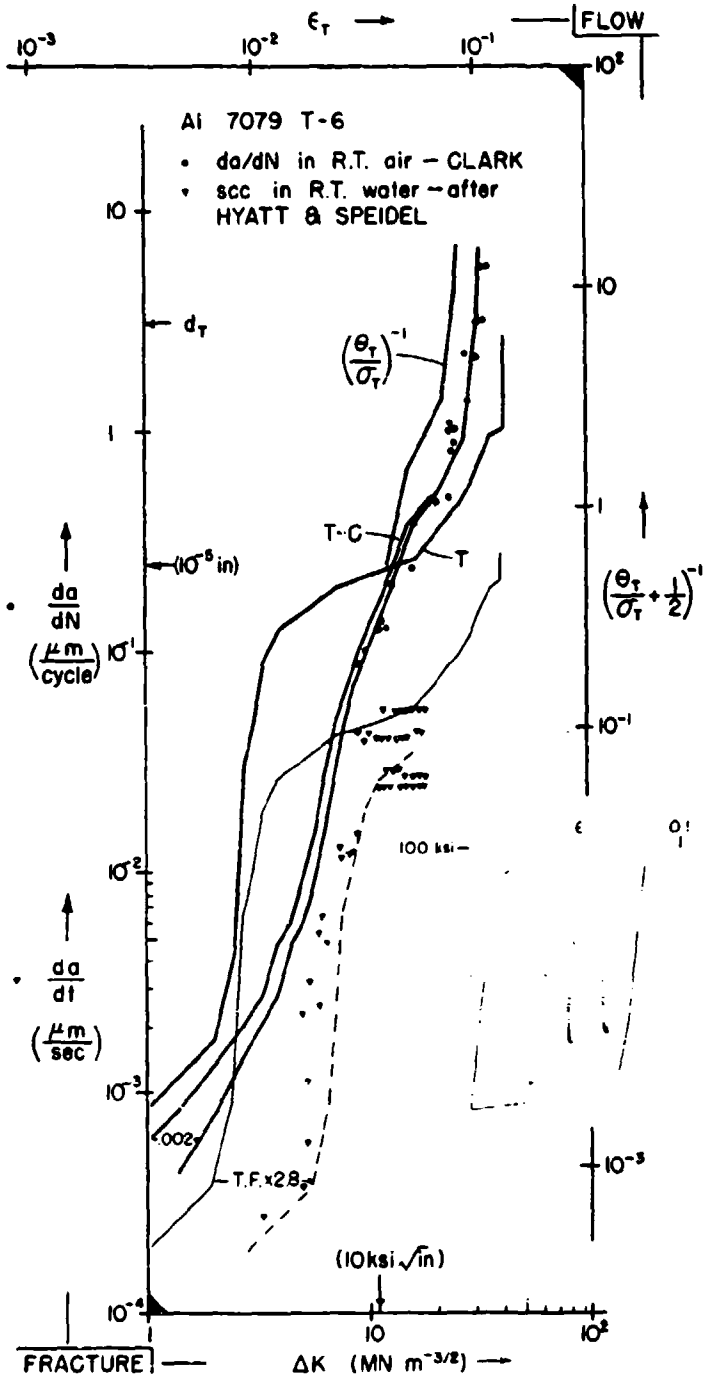

Fig. 19 - The 7079-T6 Aluminum shows somewhat more susceptibility to SCC, or higher V_S than 7075 of Fig. 18.

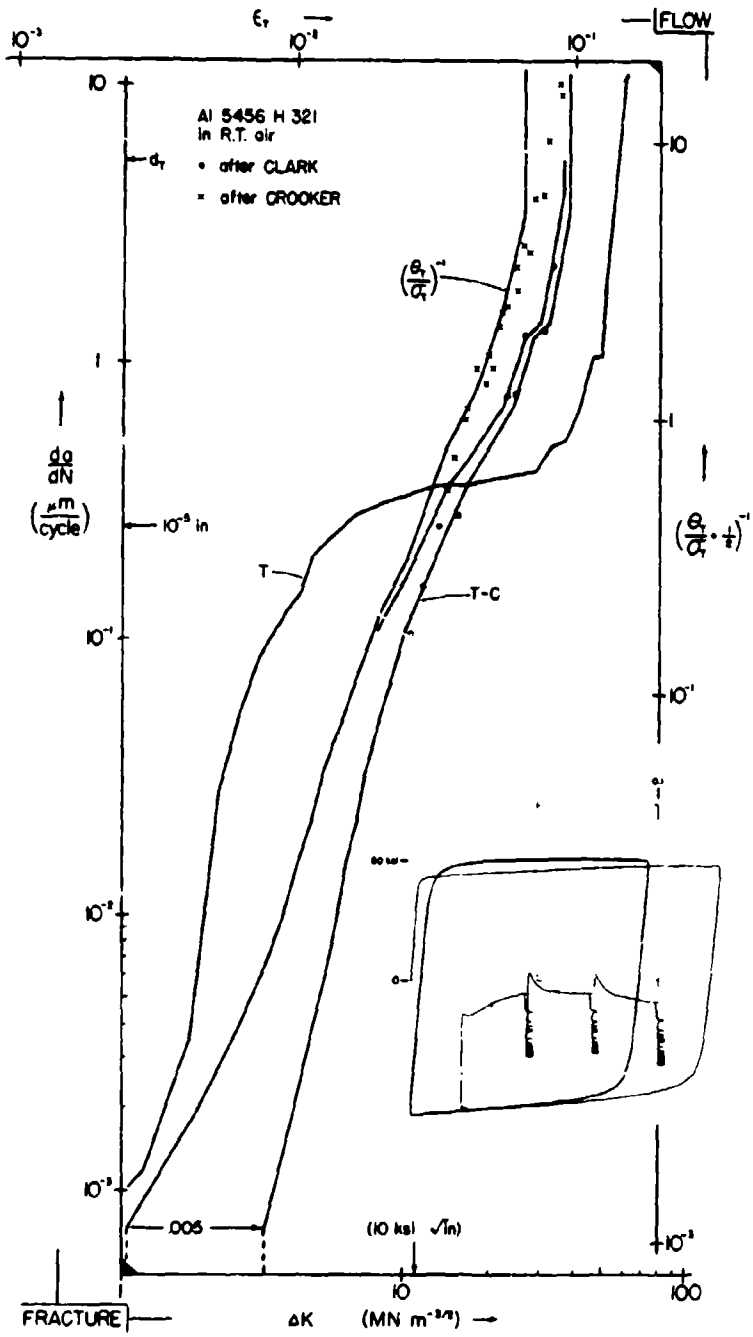

Fig. 20 - Fracture-Flow diagram for 5456-T321 Aluminum.

(Page 52 is Blank)

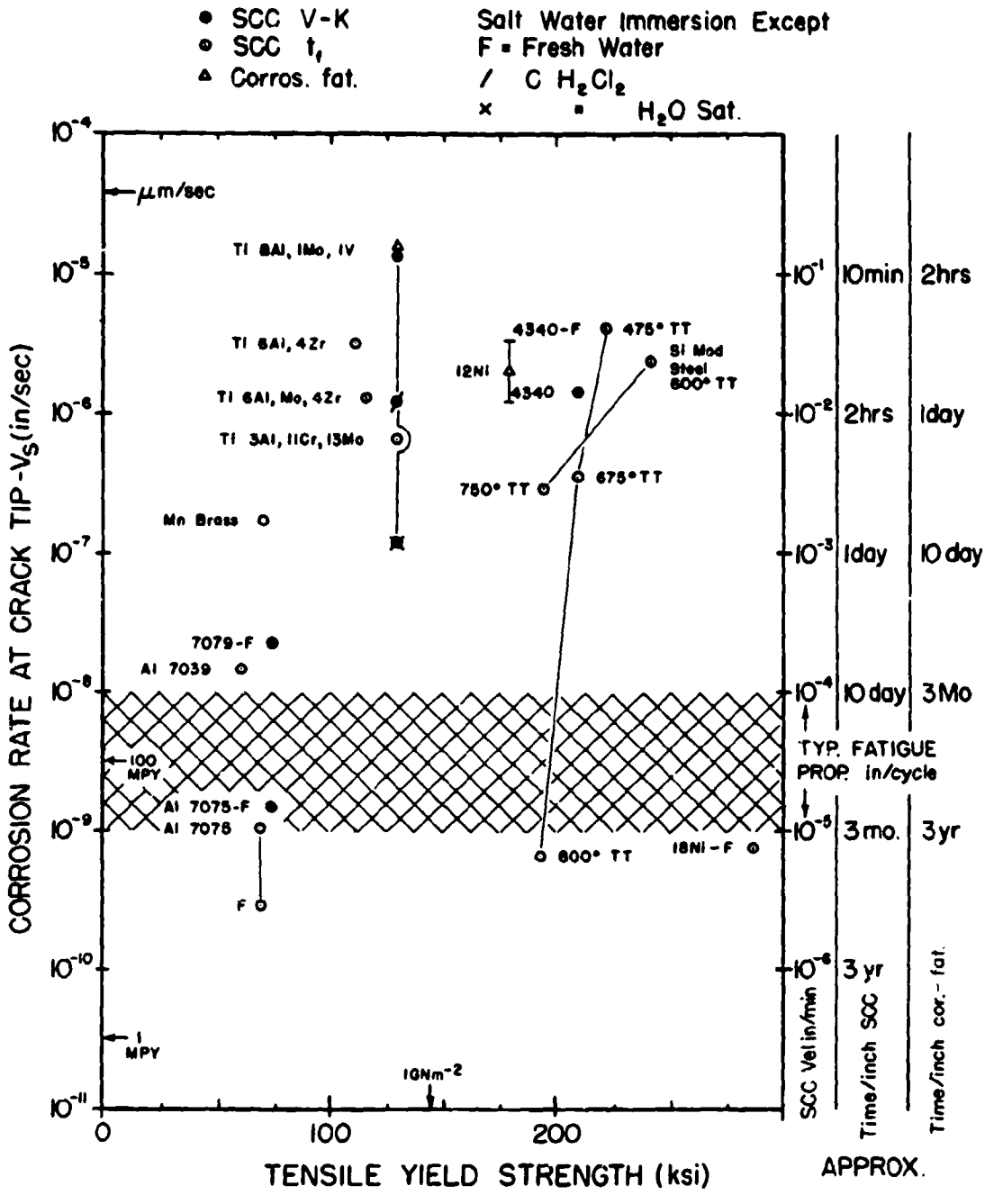

Fig. 21 - The great variability in corrosion-fatigue susceptibility (V_S) is seen in plot, vs tensile yield strength, of data from this paper as well as previous work (16). Consistency among values of V_S by different assessment methods is encouraging. For a structure loaded once a minute, V_S values above band will reduce life expectancy.